CHAPTER IV
RESULTS

4.1 Dilatometry

The CTE value that were determined from the dilatometry showed in table 7 and figure 37 for the veneering ceramics intended for use in this study, CTE ranged from the highest to the lowest value were dSIGN (12.95), CK (10.03), VM9 (9.73), emax (9.86), VM7 (7.87), and Dur (7.83) while the CTE of the Cercon® core was 10.80 μm/m·K. Glass transition temperatures (Tg) ranged from 500 °C to 620 °C that showed in table 7 and figure 38.

Table 7 The CTE value and Tg from dilatometry

Group	CTE (μm/m·K)	Glass transition temperatures (T_g) (°C)
Dur	7.83	605
VM7	7.87	620
VM9	9.73	600
CK	10.03	570
emax	9.86	500
dSIGN	12.95	515
Cercon® core	10.80	-

NB: C = Cercon® core, C-Dur = VITADur® alpha, C-VM7 = VITAVM® 7, C-VM9 = VITAVM® 9, C-CK = Cercon® ceramkiss, C-emax = IPSe.max® ceram.

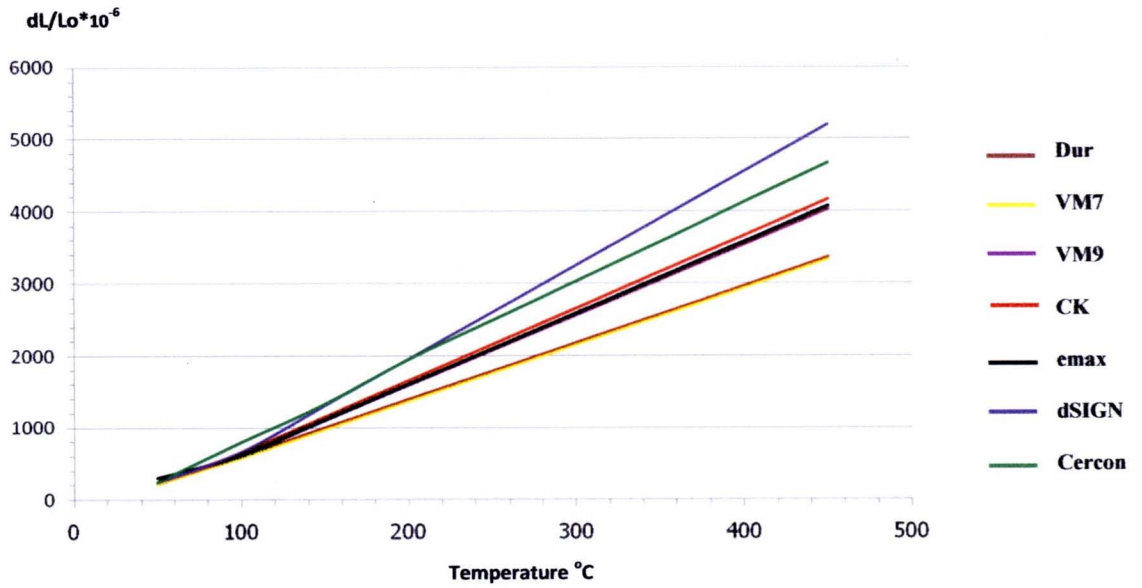

Figure 37 Linear expansion of Cercon® core and six veneering ceramics

NB: C = Cercon® core, C-Dur = VITADur® alpha, C-VM7 = VITAVM® 7, C-VM9 = VITAVM® 9, C-CK = Cercon® ceramkiss, C-emax = IPSe.max® ceram.

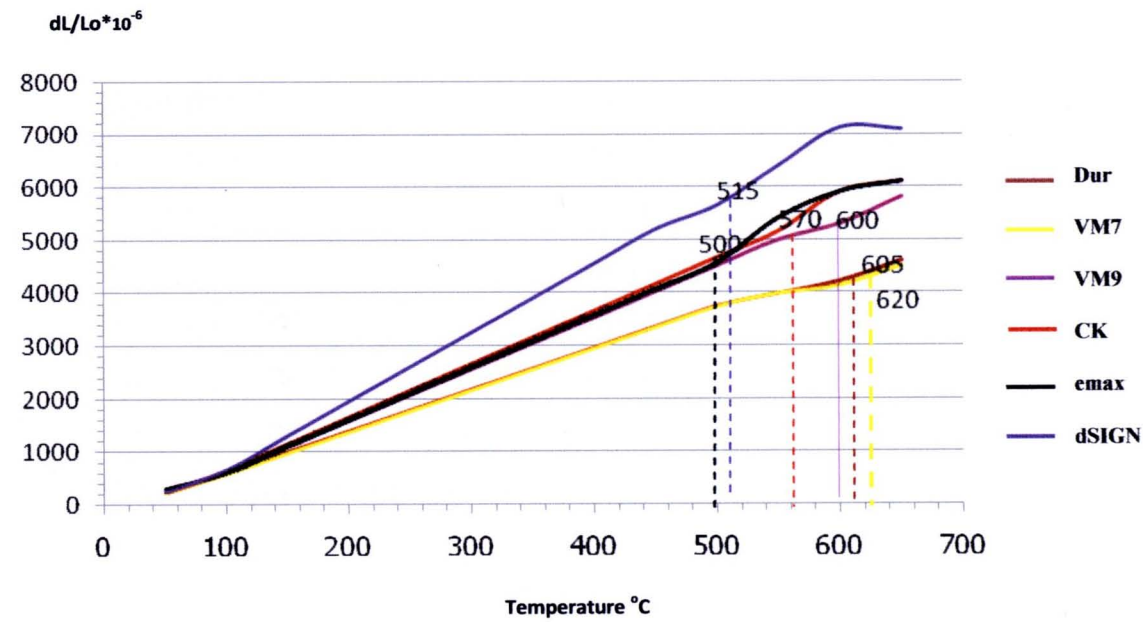

Figure 38 Tg of six veneering ceramics

NB: C = Cercon® core, C-Dur = VITADur® alpha, C-VM7 = VITAVM® 7, C-VM9 = VITAVM® 9, C-CK = Cercon® ceramkiss, C-emax = IPSe.max® ceram.

4.2 Residual stresses

4.2.1 Global residual stresses

The thermally induced global residual stresses caused by the CTE mismatch of veneering ceramic and core ceramic were determined by using the CTE and Tg from dilatometric of this study. Thermally induced global residual stresses were shown in Table 8.

Table 8 The theoretical residual stresses

Group	**Thermally induced global residual stresses** (MPa)
C-Dur	-56.44
C-VM7	-50.64
C-VM9	-20.19
C-CK	-19.28
C-emax	-12.47
C-dSIGN	+27.20

NB: C = Cercon® core, C-Dur = VITADur® alpha, C-VM7 = VITAVM®7, C-VM9 = VITAVM®9, C-CK = Cercon® ceramkiss, C-emax = IPSe.max® ceram.

4.2.2 Localized residual stresses

Upon the evaluation of the distribution of the localized residual stresses of veneering ceramic and Cercon® core, the Vickers indentation technique were used to determine residual stresses at a 300, 600 and 900 μm layer from the interface both in core and veneering layer. The residual stresses were calculated by using the formula from Kese and Rowcliffe (2003). In order to core-veneered ceramics bar sample preparation, group dSIGN were excluded from this part of study because of un-bonded of core and veneering ceramic, IPS dSIGN® that has the CTE 12.95 (Figure 39). In this situation, it means that dSIGN veneering ceramic which higher CTE from core material, will not bond on substrates. The means and standards deviation (X ± SD) of localized residual stress (MPa) in each layer both core-veneer specimens and monolithic specimens of all groups were reported in Table 9. The

means and standards deviation (X ± SD) of localized residual stress (MPa) at 300 μm layer from interface of core and veneering side of core-veneer specimens were shown in Figure 40, 41. An analysis of variance (ANOVA) was used to determine the significant difference of residual stress for each group in each layer compare to residual stress in each monolithic core and monolithic veneering porcelain indicated that there were significant difference of localized residual stress of each layer of veneering ceramic ($P < 0.05$) in all groups as shown in the tables 10.

The statistic revealed that in all groups at 300 μm from the interface of the veneering layer there were significant difference of localized residual stress and their interaction ($P < 0.05$) as shown in the tables 11 and 12. The multiple comparison of this test was shown in table 13.

The distribution of residual stresses of core and veneering ceramic of each group that were shown in Figure 43 revealed that the highest residual stress of both core and veneering ceramic were also been closely the interface, sequently.

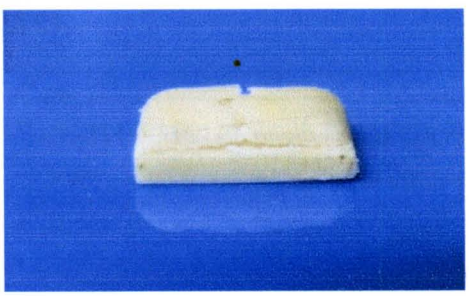

Figure 39 Un-bonded core-veneer bar specimen of group IPS dSIGN® were excluded from the part of residual stress determination

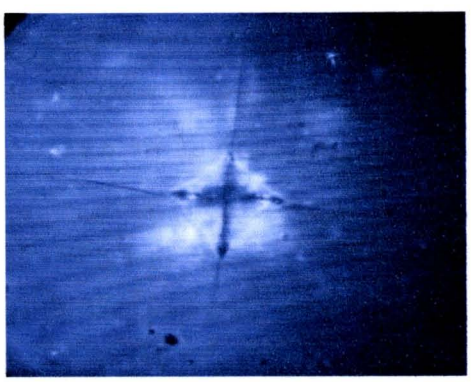

Figure 40 Show indentation crack on veneering ceramic surface

Table 9 Mean and standard deviation of localized residual stresses of core-veneered ceramic bilayer in each group and in monolithic ceramics

Group	N	Part	Localized residual stresses in core-veneered bilayer (MPa)						Localized residual stresses in monolithic (MPa)	
			300μm from interface		600μm from interface		900μm from interface		Mean ± SD	95% CI
			Mean ± SD	95% CI	Mean ± SD	95% CI	Mean ± SD	95% CI		
C-Dur	15	Core	28.347 ± 2.812	26.790 29.904	26.132 ± 2.991	24.475 27.788	25.450 ± 2.189	24.238 26.663	26.558 ± 1.192	25.897 27.218
	15	Veneer	3.351 ± 1.490	2.525 4.176	2.604 ± 1.303	1.882 3.326	2.228 ± 0.784	1.793 2.662	1.950 ± 0.321	1.771 2.128
C-VM7	15	Core	27.495 ± 1.980	26.398 28.592	25.942 ± 2.546	24.532 27.352	26.379 ± 1.955	25.296 27.462	26.558 ± 1.192	25.897 27.218
	15	Veneer	2.260 ± 0.333	2.075 2.444	1.640 ± 0.425	1.404 1.875	1.524 ± 0.380	1.313 1.735	1.433 ± 0.156	1.346 1.520
C-VM9	15	Core	26.109 ± 1.971	25.017 27.201	25.344 ± 2.075	24.194 26.493	24.518 ± 1.884	23.474 25.562	26.558 ± 1.192	25.897 27.218
	15	Veneer	2.049 ± 0.201	1.937 2.160	1.576 ± 0.211	1.458 1.693	1.632 ± 0.321	1.454 1.810	1.498 ± 0.218	1.377 1.619
C-CK	15	Core	27.396 ± 1.358	26.644 28.149	26.206 ± 1.564	25.339 27.072	26.410 ± 2.379	25.092 27.727	26.558 ± 1.192	25.897 27.218
	15	Veneer	1.790 ± 0.310	1.617 1.962	1.457 ± 0.275	1.304 1.610	1.446 ± 0.165	1.354 1.537	1.320 ± 1.284	1.284 1.357
C-emax	15	Core	27.214 ± 1.621	26.316 28.111	26.587 ± 1.440	25.789 27.384	26.056 ± 1.724	25.101 27.010	26.558 ± 1.192	25.897 27.218
	15	Veneer	2.212 ± 0.255	2.071 2.354	1.758 ± 0.144	1.678 1.838	1.740 ± 0.523	1.450 2.030	1.606 ± 0.169	1.513 1.700

NB: C = Cercon® core, C-Dur = VITADur® alpha, C-VM7 = VITAVM® 7, C-VM9 = VITAVM® 9, C-CK = Cercon® ceramkiss, C-emax = IPSe.max® ceram.

Table 10 ANOVA of localized residual stresses for each group in each layer Compare to residual stress in each monolithic core and monolithic veneering porcelain

Group		ANOVA				
		SS	**df**	**MS**	**F**	**P-value**
C-Dur (Core)	Between groups	22.407	3	7.469	1.439	0.241
	Within groups	290.743	56	5.192		
	Total	313.150	59			
C-Dur (Veneer)	Between groups	16.616	3	5.539	4.774	0.005
	Within groups	64.975	56	1.160		
	Total	81.591	59			
C-VM7 (Core)	Between groups	19.260	3	6.420	1.640	0.190
	Within groups	219.156	56	3.913		
	Total	238.416	59			
C-VM7 (Veneer)	Between groups	6.273	3	2.091	18.110	0.000
	Within groups	6.466	56	0.115		
	Total	12.739	59			
C-VM9 (Core)	Between groups	22.607	3	7.536	2.301	0.087
	Within groups	183.434	56	3.276		
	Total	206.040	59			
C-VM9 (Veneer)	Between groups	2.734	3	0.911	15.412	0.000
	Within groups	3.311	56	0.059		
	Total	6.045	59			
C-CK (Core)	Between groups	12.307	3	4.102	1.442	0.240
	Within groups	159.321	56	2.845		
	Total	171.628	59			
C-CK (Veneer)	Between groups	1.814	3	0.605	11.826	0.000
	Within groups	2.864	56	0.051		
	Total	4.678	59			
C-emax (Core)	Between groups	10.122	3	3.374	1.483	0.229
	Within groups	127.375	56	2.275		
	Total	137.497	59			
C-emax (Veneer)	Between groups	3.141	3	1.047	10.751	0.000
	Within groups	5.453	56	0.097		
	Total	8.594	59			

NB: SS = Sum of square, df = Degree of freedom, MS = Mean square, F = F-test, P-value = Probability value.

Table 11 Multiple comparisons of localized residual stress in each layer of veneer and core for each group of core-veneered compare to monolithic core and each monolithic veneering porcelain

Group	part	Layer	NS/S
C-Dur	Core	300μm from interface	I
		600μm from interface	
		900μm from interface	
		Monolithic core (Cercon®)	
	Veneer	300μm from interface	
		600μm from interface	
		900μm from interface	I
		Monolithic veneer (Dur)	
C-VM7	Core	300μm from interface	I
		600μm from interface	
		900μm from interface	
		Monolithic core (Cercon®)	
	Veneer	300μm from interface	
		600μm from interface	
		900μm from interface	I
		Monolithic veneer (VM7)	
C-VM9	Core	300μm from interface	I
		600μm from interface	
		900μm from interface	
		Monolithic core (Cercon®)	
	Veneer	300μm from interface	
		600μm from interface	
		900μm from interface	I
		Monolithic veneer (VM9)	
C-CK	Core	300μm from interface	I
		600μm from interface	
		900μm from interface	
		Monolithic core (Cercon®)	
	Veneer	300μm from interface	
		600μm from interface	
		900μm from interface	I
		Monolithic veneer (CK)	
C-emax	Core	300μm from interface	I
		600μm from interface	
		900μm from interface	
		Monolithic core (Cercon®)	
	Veneer	300μm from interface	
		600μm from interface	
		900μm from interface	I
		Monolithic veneer (emax)	

NB: C = Cercon® core, C-Dur = VITADur® alpha, C-VM7 = VITAVM® 7, C-VM9 = VITAVM® 9, C-CK = Cercon® ceramkiss, C-emax = IPSe.max® ceram.

I = *NS* ($P \geq 0.05$)

Table 12 ANOVA of localized residual stresses of the 1st layer (300μm from interface) both in the core and veneering porcelain part among each group

Group		ANOVA				
		SS	**df**	**MS**	**F**	**P-value**
Veneer	Between groups	21.482	4	5.370	10.588	0.000
	Within groups	35.506	70	0.507		
	Total	56.988	74			
Core	Between groups	38.531	4	9.633	2.385	0.059
	Within groups	282.699	70	4.039		
	Total	321.230	74			

NB: SS = Sum of square, df = Degree of freedom, MS = Mean square, F = F-test, P-value = Probability value.

Table 13 Multiple comparisons of localized residual stress of the 1st layer (300μm from interface) both in the core and veneering porcelain part among each group

Multiple comparison of the 1st layer in veneer	Group	V_1^{st}-Dur	V_1^{st}-VM7	V_1^{st}-VM9	V_1^{st}-CK	V_1^{st}-emax
	V_1^{st}-Dur		1.091	1.302*	1.561*	1.138
	V_1^{st}-VM7			0.210	0.470*	0.047
	V_1^{st}-VM9				0.259	0.163
	V_1^{st}-CK					0.422*
	V_1^{st}-emax					
Multiple comparison of the 1st layer in core	Group	C_1^{st}-Dur	C_1^{st}-VM7	C_1^{st}-VM9	C_1^{st}-CK	C_1^{st}-emax
	C_1^{st}-Dur		0.852	2.238	0.950	1.133
	C_1^{st}-VM7			1.386	0.098	0.281
	C_1^{st}–VM9				1.287	1.104
	C_1^{st}–CK					0.182
	C_1^{st}-emax					

NB: C = Cercon® core, C-Dur = VITADur® alpha, C-VM7 = VITAVM®7, C-VM9 = VITAVM®9, C-CK = Cercon® ceramkiss, C-emax = IPSe.max® ceram.

The Mean and standard deviation of the difference between localized residual stress in 1st layer (300 μm from interface) and in monolithic of both veneer and core side of each group were shown in table 14. The statistic revealed that have difference between localized residual stress in 1st layer (300 μm from interface) and in monolithic of veneer side were significant difference of and their interaction ($P< 0.05$) and the multiple comparison were shown in table 15 and 16.

Table 14 The Mean and standard deviation of difference between residual stress in 1st layer and in monolithic of both veneer and core

Group	N	Cercon® core layer side		Veneering ceramic layers side	
		Δ residual stress (MPa) (1st layer – monolithic)		Δ residual stress (MPa) (1st layer – monolithic)	
		Mean	SD	Mean	SD
C-Dur	15	2.117	1.576	1.396	1.235
C-VM7	15	2.362	1.196	0.922	0.374
C-VM9	15	2.086	1.410	0.371	0.300
C-CK	15	1.793	1.028	0.476	0.325
C-emax	15	1.470	0.872	0.602	0.274

NB: C = Cercon® core, C-Dur = VITADur® alpha, C-VM7 = VITAVM®7, C-VM9 = VITAVM®9, C-CK = Cercon® ceramkiss, C-emax = IPSe.max® ceram.

Table 15 ANOVA of difference between residual stress in 1st layer and in monolithic both in the core and veneering porcelain part among each group

Group		ANOVA				
		SS	df	MS	F	P-value
Core	Between groups	7.039	4	1.760	1.139	0.345
	Within groups	108.161	70	1.545		
	Total	115.201	74			
Veneer	Between groups	10.324	4	2.581	6.661	0.000
	Within groups	27.126	70	0.388		
	Total	37.450	74			

NB: SS = Sum of square, df = Degree of freedom, MS = Mean square, F = F-test, P-value = Probability value.

Table 16 Multiple comparisons of difference between residual stress in 1st layer and in monolithic both in the core and veneering porcelain part among each group

	Group	C_1^{st}-Dur	C_1^{st}-VM7	C_1^{st}-VM9	C_1^{st}-CK	C_1^{st}-emax
Multiple comparison of the 1st layer in core	C_1^{st}-Dur		0.2447	0.031	0.324	0.646
	C_1^{st}-VM7			0.276	0.568	0.891
	C_1^{st}–VM9				0.292	0.615
	C_1^{st}-CK					0.322
	C_1^{st}-emax					
	Group	V_1^{st}-Dur	V_1^{st}-VM7	V_1^{st}-VM9	V_1^{st}-CK	V_1^{st}-emax
Multiple comparison of the 1st layer in veneer	V_1^{st}-Dur		0.474	1.025	0.920	0.794
	V_1^{st}-VM7			0.551*	0.446*	0.320
	V_1^{st}-VM9				0.104	0.230
	V_1^{st}-CK					0.126
	V_1^{st}-emax					

NB: C = Cercon® core, C-Dur = VITADur® alpha, C-VM7 = VITAVM®7, C-VM9 = VITAVM®9, C-CK = Cercon® ceramkiss, C-emax = IPSe.max® ceram.

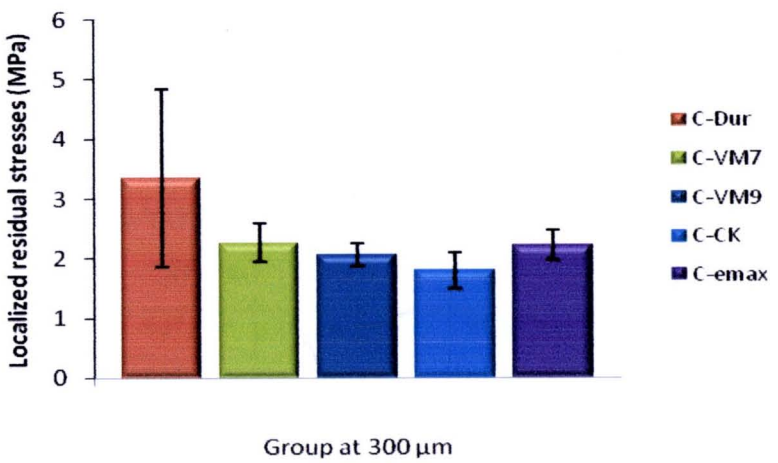

Figure 41 Bar graph of the mean localized residual stresses and standard deviation at 300 µm from interface in veneer side of core-veneer specimens

NB: C = Cercon® core, C-Dur = VITADur® alpha, C-VM7 = VITAVM®7, C-VM9 = VITAVM®9, C-CK = Cercon® ceramkiss, C-emax = IPSe.max® ceram.

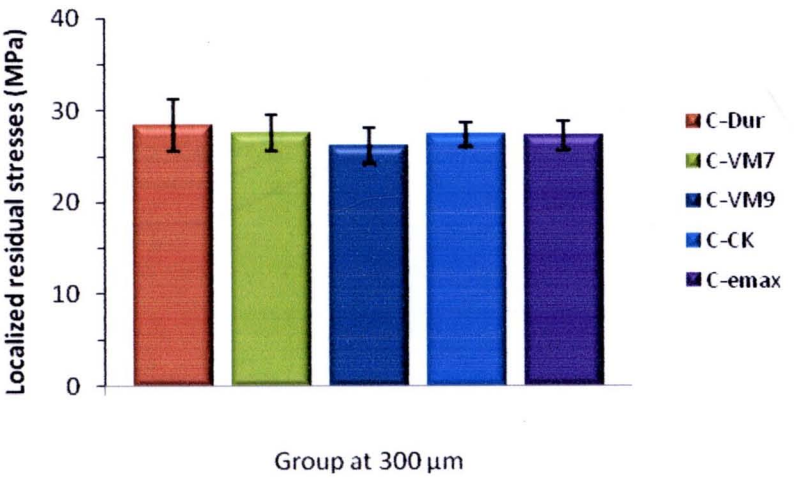

Figure 42 Bar graph of the mean localized residual stresses and standard deviation at300 µm from interface in core side of core-veneer specimens

NB: C = Cercon® core, C-Dur = VITADur® alpha, C-VM7 = VITAVM® 7, C-VM9 = VITAVM® 9, C-CK = Cercon® ceramkiss, C-emax = IPSe.max® ceram.

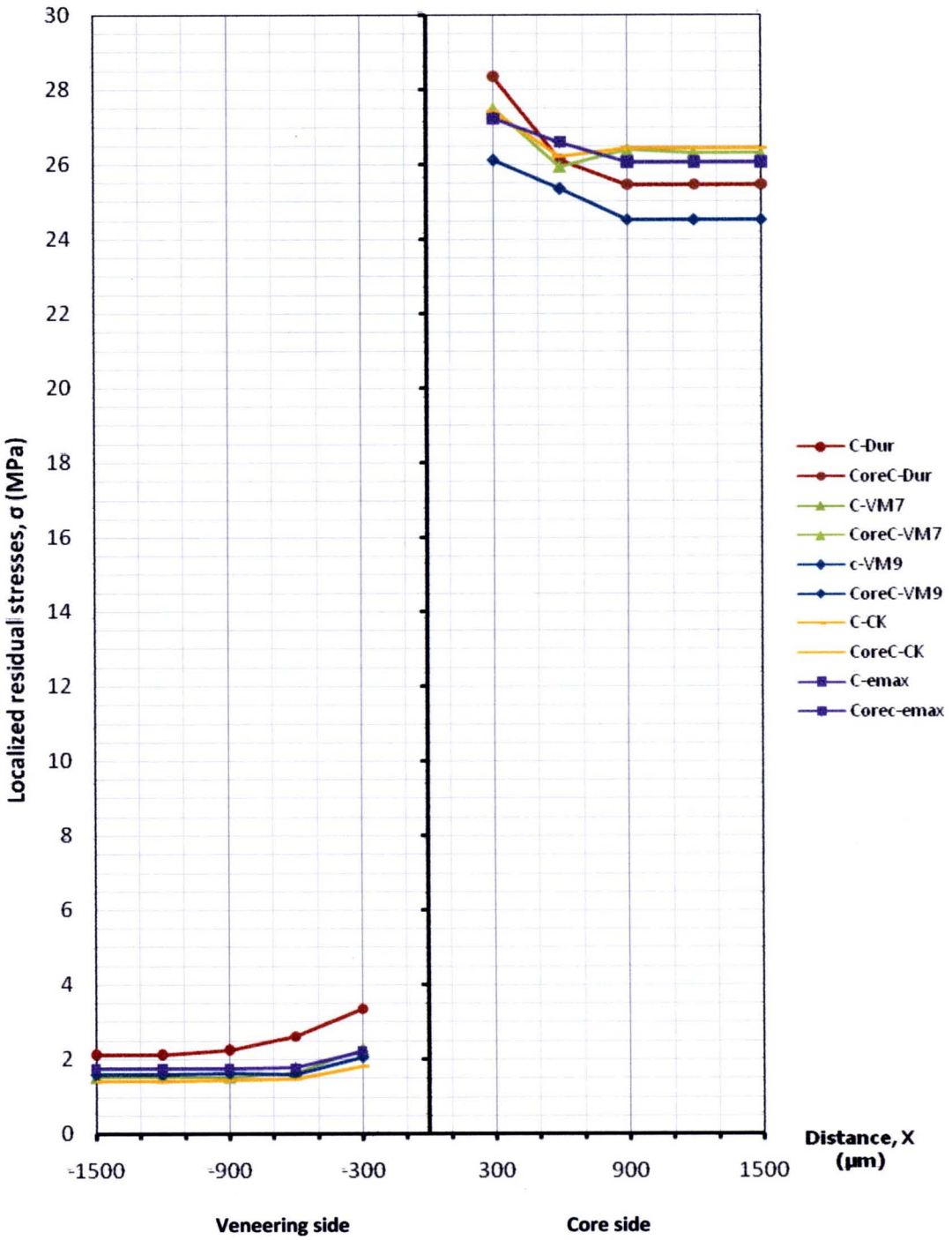

Figure 43 Distribution of localized residual stress in each group both on the veneer and core side

NB: C = Cercon® core, C-Dur = VITADur® alpha, C-VM7 = VITAVM® 7, C-VM9 = VITAVM® 9, C-CK = Cercon® ceramkiss, C-emax = IPSe.max® ceram.

4.2.8 The theoretical thermally induced global residual stresses.

The comparison of theoretical residual stress and experimental residual stress at 300μm from interface both veneer and core side, from Vickers indentation testing, were shown in table 22 and figure 44.

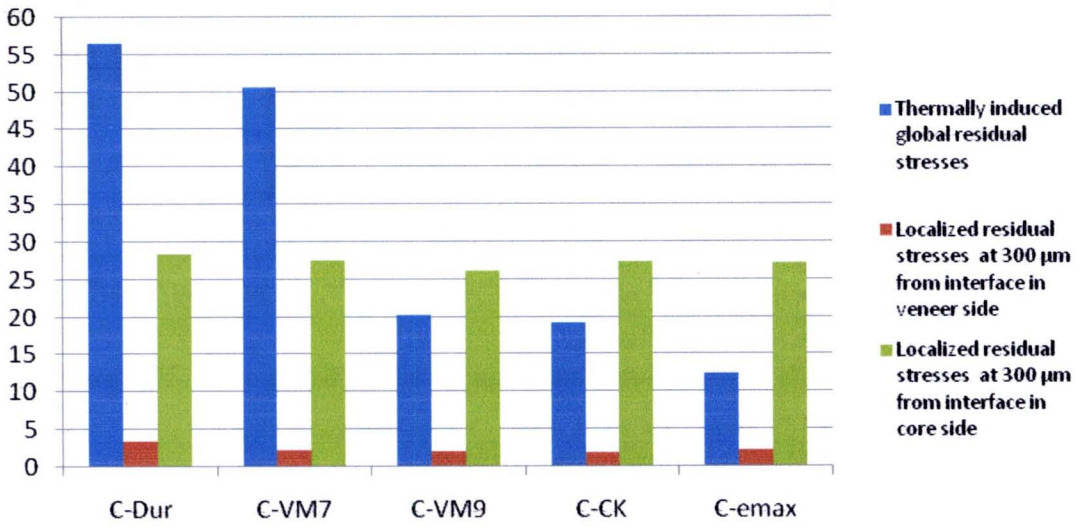

Figure 44 Bar graph of the thermally induced global residual stresses and localized residual stress at near interface (300 μm from interface)

NB: C = Cercon® core, C-Dur = VITADur® alpha, C-VM7 = VITAVM®7, C-VM9 = VITAVM®9, C-CK = Cercon® ceramkiss, C-emax = IPSe.max® ceram.

4.3 Shear bond strength

The results of the shear bond strength tested were reported in terms of the mean and standard deviation (X ± SD) of shear bond strength as shown in Table 17 and graph in figures 45. An analysis of variance (ANOVA) and Tamhane's multiple comparison were evaluated and indicated that there were significant difference of shear bond strength of IPSe.max®ceram from VITAVM®9 ($P < 0.05$) and their interaction ($P < 0.05$) as shown in the tables 18 and 19. This indicated that the varied coefficient of thermal expansion of the ceramic influence significantly to the shear bond strength (SBS) at 95% level of confidence.

Table 17 Mean shear bond strength (SBS) and standard deviation of each group

Group abbreviate	N	Shear bond strength (MPa)		95% Confidence Interval for Mean	
		Mean	SD	Lower Bound	Upper Bound
C-Dur	15	22.5527	5.1438	19.7041	25.4012
C-VM7	15	19.7460	7.1739	15.7732	23.7188
C-VM9	15	25.8560	2.7432	24.3368	27.3752
C-CK	15	25.4187	4.9019	22.7041	28.1333
C-emax	15	19.9400	5.2838	17.0139	22.8661

NB: C = Cercon® core, C-Dur = VITADur® alpha, C-VM7 = VITAVM®7, C-VM9 = VITAVM®9, C-CK = Cercon® ceramkiss, C-emax = IPSe.max® ceram.

Table 18 ANOVA of shear bond strength (SBS)

	SS	df	MS	F	P-value
Between Groups	505.753	4	126.438	4.601	.002
Within Groups	1923.565	70	27.479		
Total	2429.318	74			

NB: SS = Sum of square, df = Degree of freedom, MS = Mean square, F = F-test, P-value = Probability value.

Table 19 Tamhane's pairwise comparisons of shear bond strength

Group	C-Dur	C-VM7	C-VM9	C-CK	C-emax
C-Dur		0.980	0.453	0.875	0.950
C-VM7			0.092	0.241	1.000
C-VM9				1.000	0.014*
C-CK					0.093
C-emax					

NB: C = Cercon® core, C-Dur = VITADur® alpha, C-VM7 = VITAVM®7, C-VM9 = VITAVM®9, C-CK = Cercon® ceramkiss, C-emax = IPSe.max® ceram.

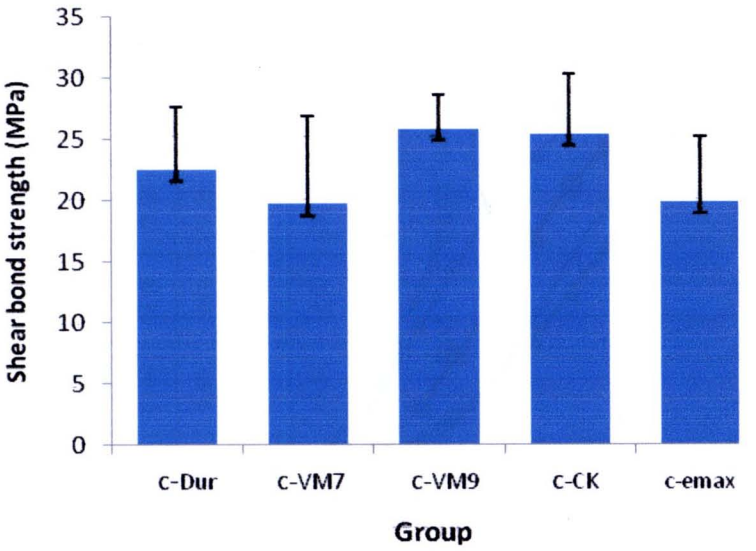

Figure 45 Bar graph of the mean shear bond strength and standard deviation

NB: C = Cercon® core, C-Dur = VITADur® alpha, C-VM7 = VITAVM®7, C-VM9 = VITAVM®9, C-CK = Cercon® ceramkiss, C-emax = IPSe.max® ceram.

The Weibull analysis of shear bond strength (SBS) which include the Weibull modulus, characteristic strength, the of probabilities of survival under shear bond strength of 5, 9, 13, 17, 21, 25, 29, and 33 MPa were showed in table 20, figures 46, 47.

Weibull modulus can be ranked from highest to lowest as follows: C-CK (5.53), C-Dur (4.49), C-VM7 (2.93), C-emax (3.94), and C-VM9 (8.86).

The characteristic shear bond strength (SBS) that was ranks from the highest to the lowest value were group C-VM9 (27.77), C-CK (25.06), C-Dur (22.12), C-emax (19.34), and C-VM7 (18.69).

All groups of Cercon® core had the probabilities of survival greater than 80 percent at the shear bond strength level of 9 MPa. At the shear bond strength level of 25 MPa, they were ranked from highest to lowest as follows: C-VM9 (46.68), C-CK (37.30), C-Dur (17.70), C-emax (6.40) and C-VM7 (9.58).

The stress level required for 99, 95, 90, 85, 15, 10 and 5 percent probabilities of survival for each group followed table 18 reveal that shear bond strength level with a 95 percent probability of survival ranked from highest to lowest as follows: C-CK (14.66), C-Dur (11.42), C-VM7 (6.78), C-emax (9.11) and C-VM9 (18.43).

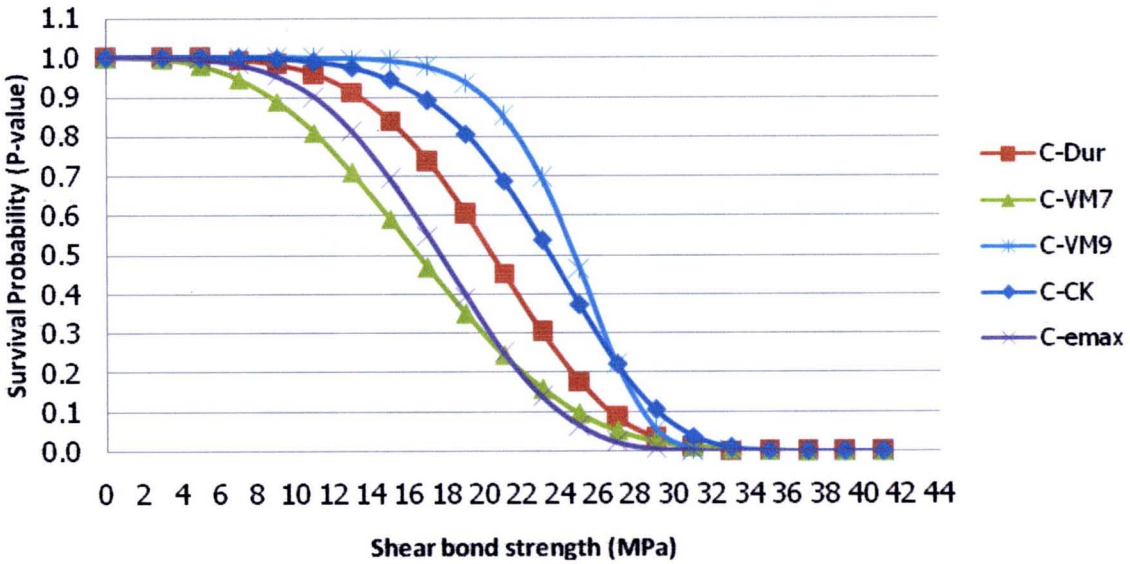

Figure 46 Relative Weibull analysis curves among Cercon® core for each group

NB: C = Cercon® core, C-Dur = VITADur® alpha, C-VM7 = VITAVM® 7, C-VM9 = VITAVM® 9, C- CK = Cercon® ceramkiss, C-emax = IPSe.max® ceram.

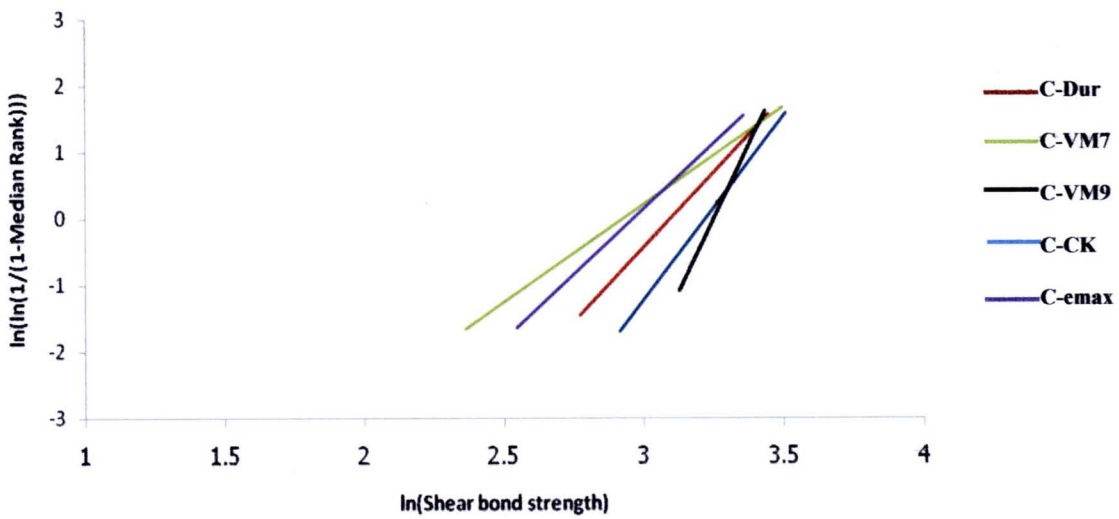

Figure 47 Line fit plot among Cercon® for each group

NB: C = Cercon® core, C-Dur = VITADur® alpha, C-VM7 = VITAVM® 7, C-VM9 =VITAVM® 9, C-CK = Cercon® ceramkiss, C-emax = IPSe.max® ceram.

Table 20 Weibull analysis and probabilities of survival of shear bond strength

Group abbreviate	N	Weibull Modulus (m)	Characteristic Strength (σ^0)	Probabilities of survival at stress of 5, 9, 13, 17, 21, 25, 29, 33 (MPa)								Stress level of 99%,95%,90%,85%,15%,10% and 5% probabilities of survival (MPa)						
				5	9	13	17	21	25	29	33	99%	95%	90%	85%	15%	10%	5%
C-Dur	15	4.49	22.12	99.87	98.23	91.23	73.62	45.33	17.70	3.42	0.24	7.94	11.42	13.40	14.76	25.51	26.63	28.24
C-VM7	15	2.93	18.69	97.92	88.91	70.81	46.88	24.49	9.58	2.67	0.50	3.88	6.78	8.67	10.05	23.25	24.84	27.17
C-VM9	15	8.86	27.77	99.99	99.99	99.76	97.53	85.00	46.68	5.85	0.01	15.34	18.43	19.99	21.00	27.71	28.32	29.17
C-CK	15	5.53	25.06	99.99	99.66	97.40	89.01	68.70	37.30	10.60	1.02	10.92	14.66	16.69	18.05	28.13	29.13	30.55
C-emax	15	3.94	19.34	99.52	95.23	81.19	54.86	25.11	6.40	0.71	0.02	6.02	9.11	10.93	12.20	22.75	23.90	25.55

NB: C = Cercon® core, C-Dur = VITADur® alpha, C-VM7 = VITAVM® 7, C-VM9 = VITAVM® 9, C-CK = Cercon® ceramkiss, C-emax = IPSe.max® ceram.

4.4 Regression analysis

4.4.1 Relation between bond strength and residual stresses

Linear regression analysis was used to assess the relation between bond strength and localized residual stress near the interface and the results were shown in tables 21 to 24 and figures 48 to 50.

Table 21 Model Summary(b)

Model	R	R Square	Adjusted R Square	Std. Error of the Estimate
1	.267(a)	.071	.058	2.11225

a Predictors: (Constant), SBS
b Dependent Variable: CTE

Table 22 Coefficients(a)

Model		Unstandardized Coefficients		Standardized Coefficients	t	Sig.
		B	Std. Error	Beta		
1	(Constant)	29.657	1.003		29.567	.000
	SBS	-.101	.043	-.267	-2.363	.021

a Dependent Variable: CTE

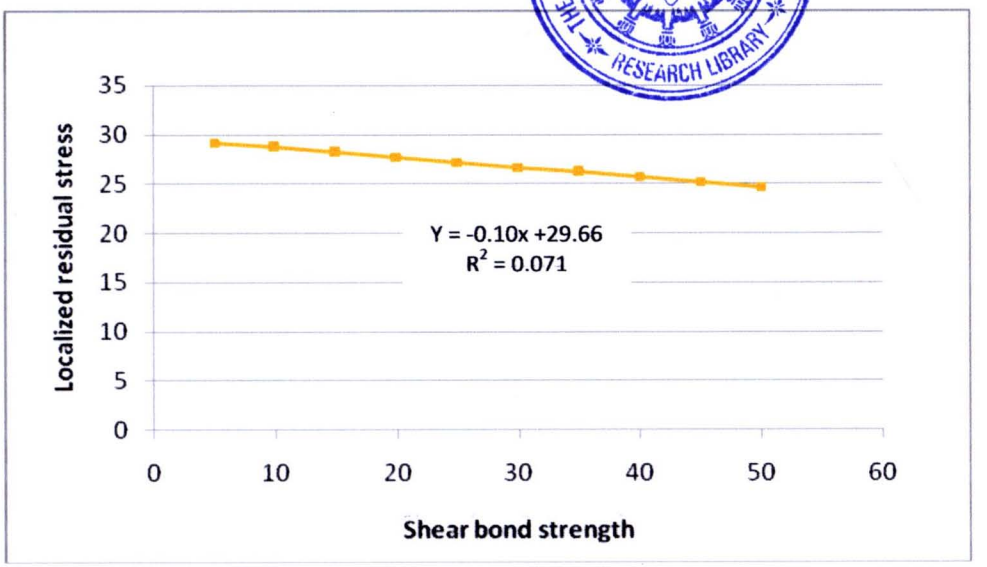

Figure 48 The linear regression of the scatter plot of bond strength and localized residual stresses near the interface of core, depicted linear profile with low R^2.

(NB: X = shear bond strength, Y = localized residual stress)

Table 23 Model Summary(b)

Model	R	R Square	Adjusted R Square	Std. Error of the Estimate
1	.000(a)	.000	-.014	.88367

a Predictors: (Constant), SBS
b Dependent Variable: CTE

Table 24 Coefficients(a)

Model		Unstandardized Coefficients		Standardized Coefficients	t	Sig.
		B	Std. Error	Beta		
1	(Constant)	2.333	.420		5.560	.000
	SBS	-2.927E-05	.018	.000	-.002	.999

a Dependent Variable: CTE

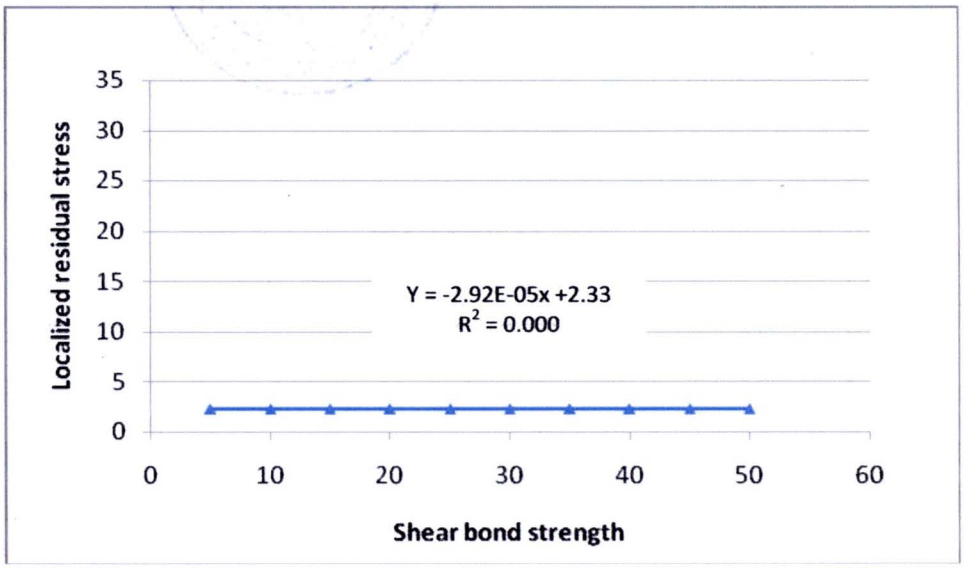

Figure 49 The linear regression of the scatter plot of bond strength and localized residual stresses near the interface of veneering ceramic, depicted linear profile with $R^2 = 0$.

(NB: X = shear bond strength, Y = localized residual stress)

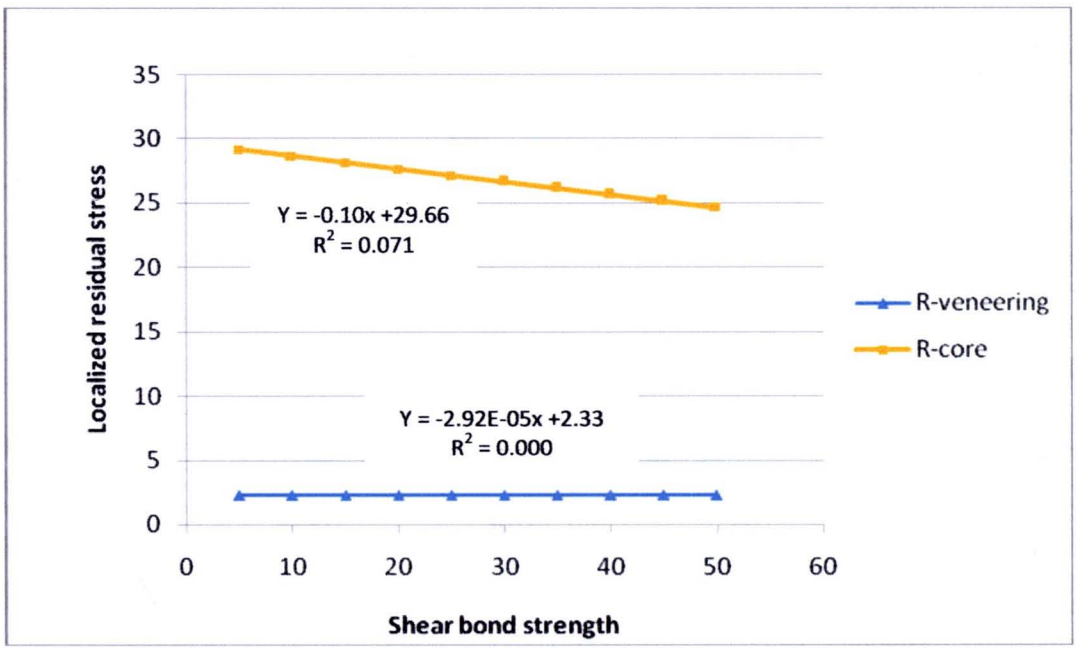

Figure 50 The comparing linear regression of the scatter plot of bond strength and localized residual stresses near the interface of core and veneering ceramic

(NB: X = shear bond strength, Y = localized residual stress)

4.4.2 Relation between bond strength and CTE difference

From linear regression analysis shown in tables 25 to 26 and figure 51, there was no linear relationship between bond strength and difference CTE.

Table 25 Model Summary(b)

Model	R	R Square	Adjusted R Square	Std. Error of the Estimate
1	.220(a)	.048	.035	.98464

a Predictors: (Constant), SBS
b Dependent Variable: CTE

Table 26 Coefficients(a)

Model		Unstandardized Coefficients		Standardized Coefficients	t	Sig.
		B	Std. Error	Beta		
1	(Constant)	2.611	.468		5.584	.000
	SBS	-.039	.020	-.220	-1.929	.058

a Dependent Variable: CTE

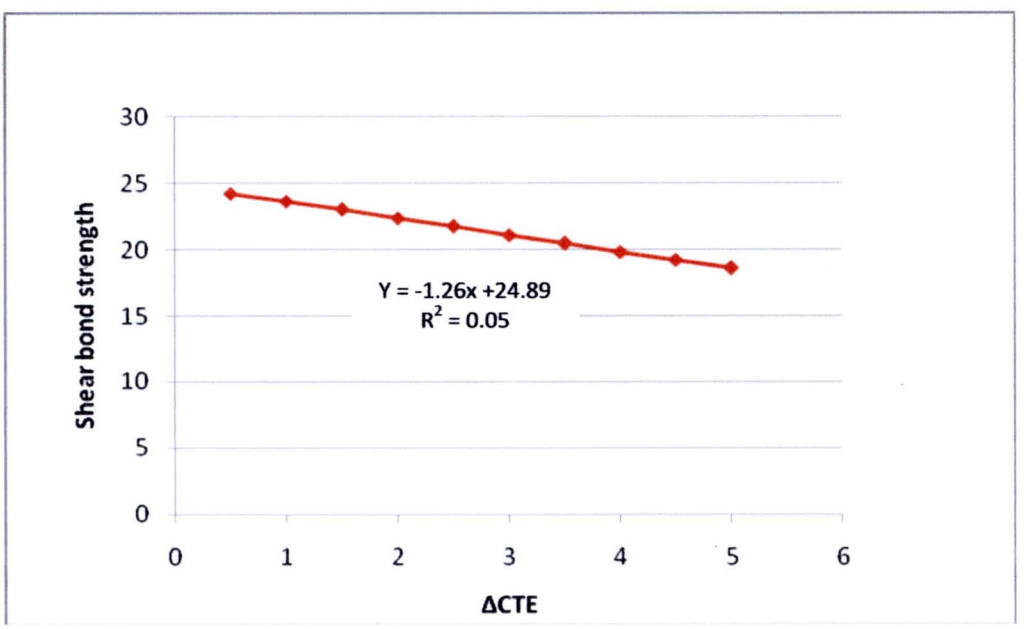

Figure 51 The linear regression of the scatter plot of ΔCTE and bond strength, depicted linear profile with low R^2.

(NB: X = shear bond strength, Y = localized residual stress)

4.5 Scanning electron micrographs

The microstructures of the specimens from each group were investigated by observation both at the fracture surface area in veneering side of Cercon® core and veneering ceramic. The scanning electron micrographs of the fracture site for each group were shown in figures 52, 53, 55, 56, 58, 59, 61, 62, 64, 65, 67, and 68 in (a) to (d) at the magnification of ×500, ×1000, ×2000 and ×4000 respectively. The fracture surface of the Cercon® core ceramic in each group were further evaluated by etching the fracture surface prior to examine through the scanning electron microscope. The photomicrographs of the etched surfaces of the fracture site were shown in figures 52, 53, 55, 56, 58, 59, 61, 62, 64, 65, 67, and 68 in (e) to (f) at the magnification of ×4000 and ×10000 respectively.

The scanning electron micrographs of the interface of core-veneer specimens were shown in figures 54, 57, 60, 63, 66 and 69 in (a) to (f) at the magnification of ×50, ×100, ×200, ×500, ×1000 and ×2000 respectively.

The scanning electron micrographs of the fracture surface area in veneering side of the Cercon® core ceramic that were shown in the figures 52, 55, 58, 61, 64 and 67 in (a) to (d) revealed that there was not fracture of the inside of core or veneering ceramic, also cohesive failure was not occurred.

The scanning electron micrographs of the fracture surface area in veneering side of the veneering ceramic that were shown in the figures 53, 56, 59, 62, 65 and 68 in (a) to (d), as the same manner of completed fracture in fracture surface area in veneering side of the Cercon® core ceramic.

The scanning electron micrographs of the interface of core-veneer specimens of all groups shown that there were bond of the core and veneering ceramic, except IPS dSIGN® there was microgap at the core-veneered interface as seen in figure 69.

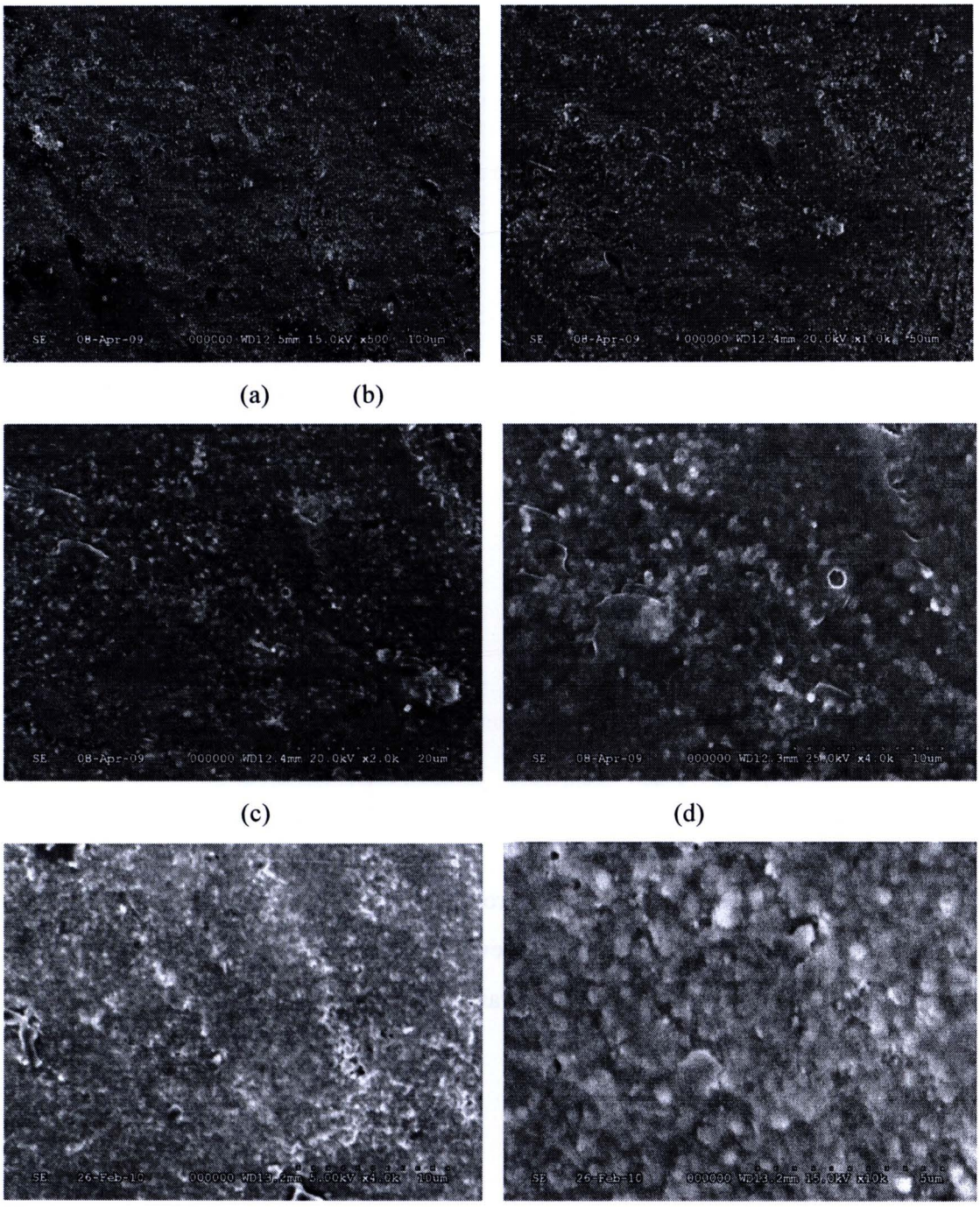

Figure 52 SEM photomicrographs of group Dur (Cercon®core ceramic veneering with VITA DurAlpha) that reveals fracture core-veneer at the fracture surface of core structure upon (a)X500, (b)X1000, (c)X2000, (d)X4000 magnification and reveals the etched fracture surface of ceramic core at (e)X4000 and (f)X10000 magnification

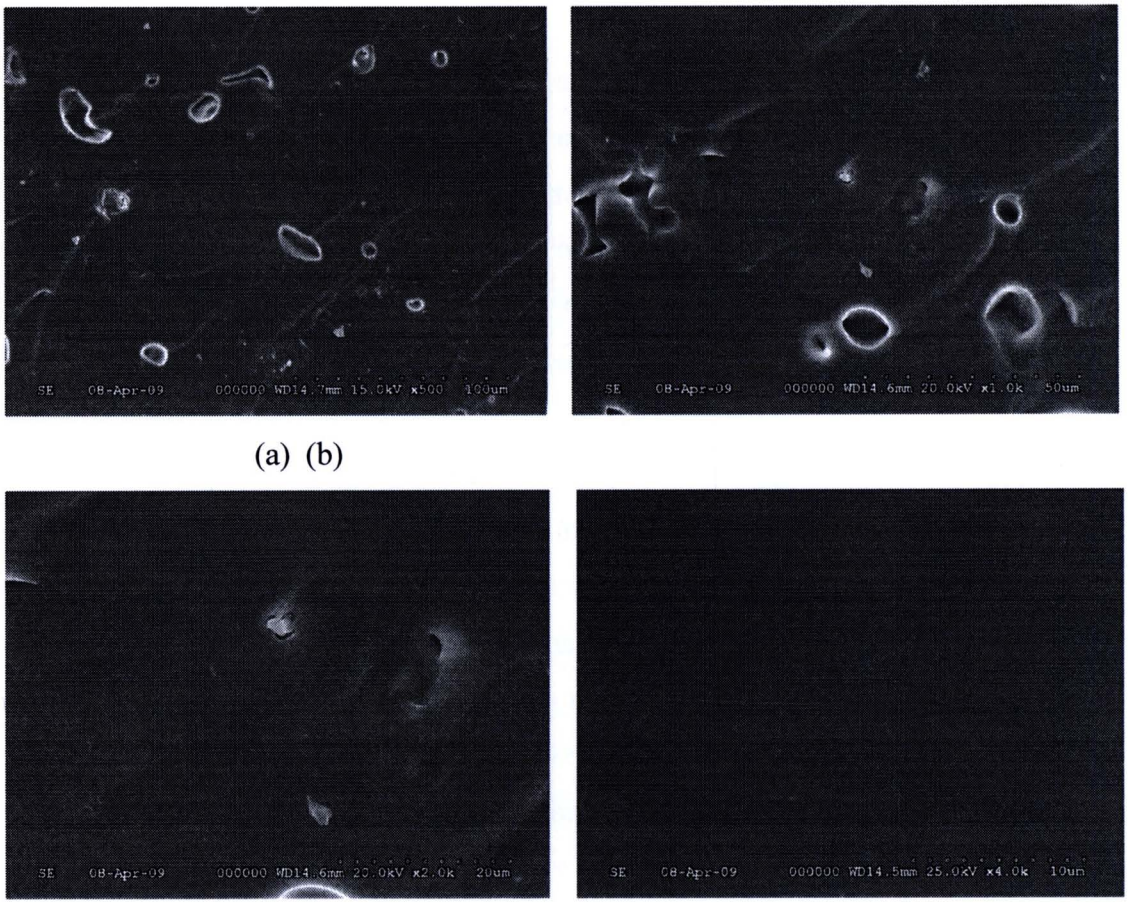

Figure 53 SEM photomicrographs of group Dur (Cercon®core ceramic veneering with VITA DurAlpha) that reveals fracture core-veneer at the fracture surface of Dur veneering ceramic upon (a)X500, (b)X1000, (c)X2000, (d)X4000 magnification

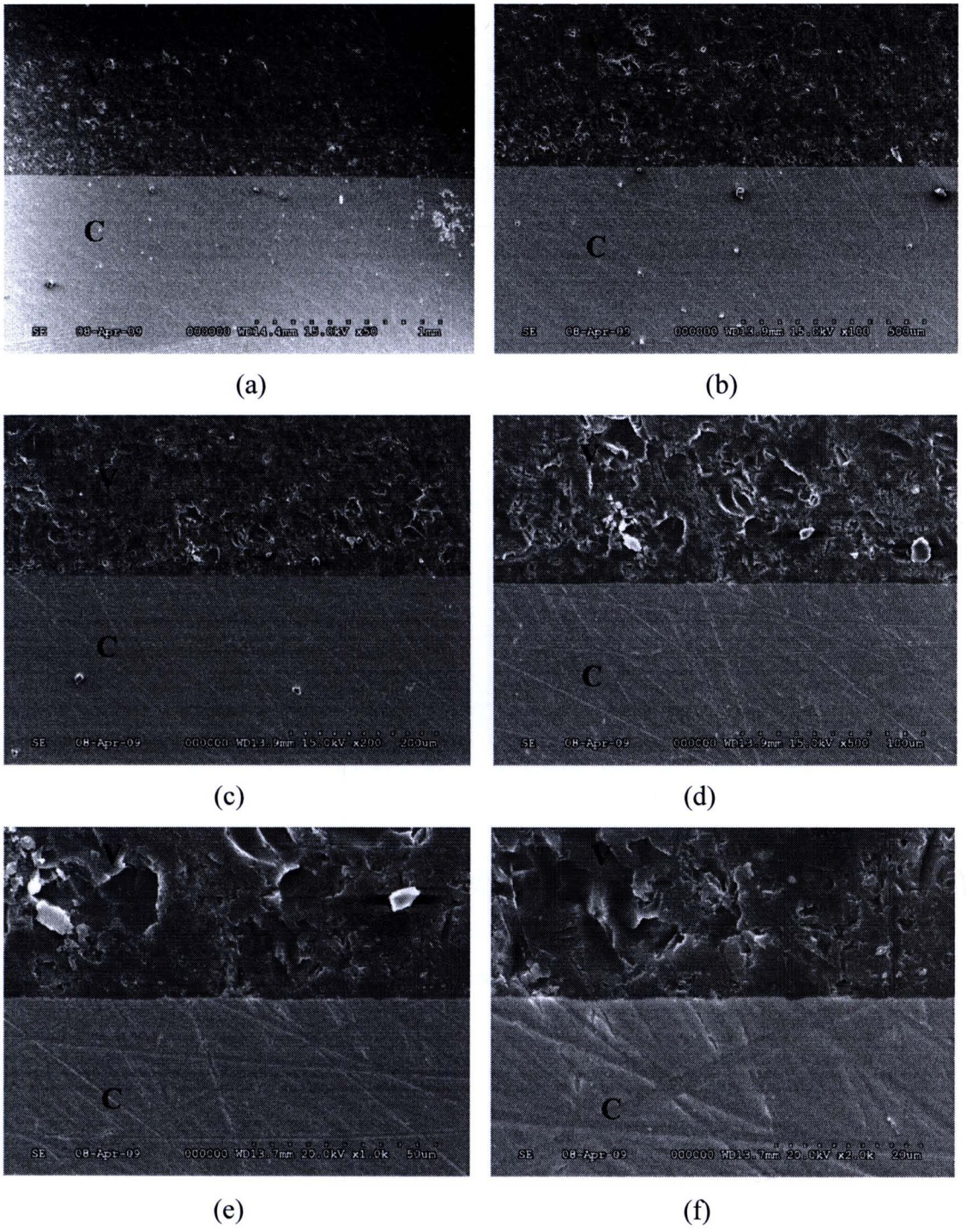

Figure 54 SEM photomicrographs of group Dur (Cercon® core ceramic veneering with VITA DurAlpha) that reveals the core-veneer interface at (a)X50, (b)X100, (c)X200, (d)X500, (e)X1000, (f)X2000 magnification.

NB: V = Veneering ceramic, C = Cercon® core.

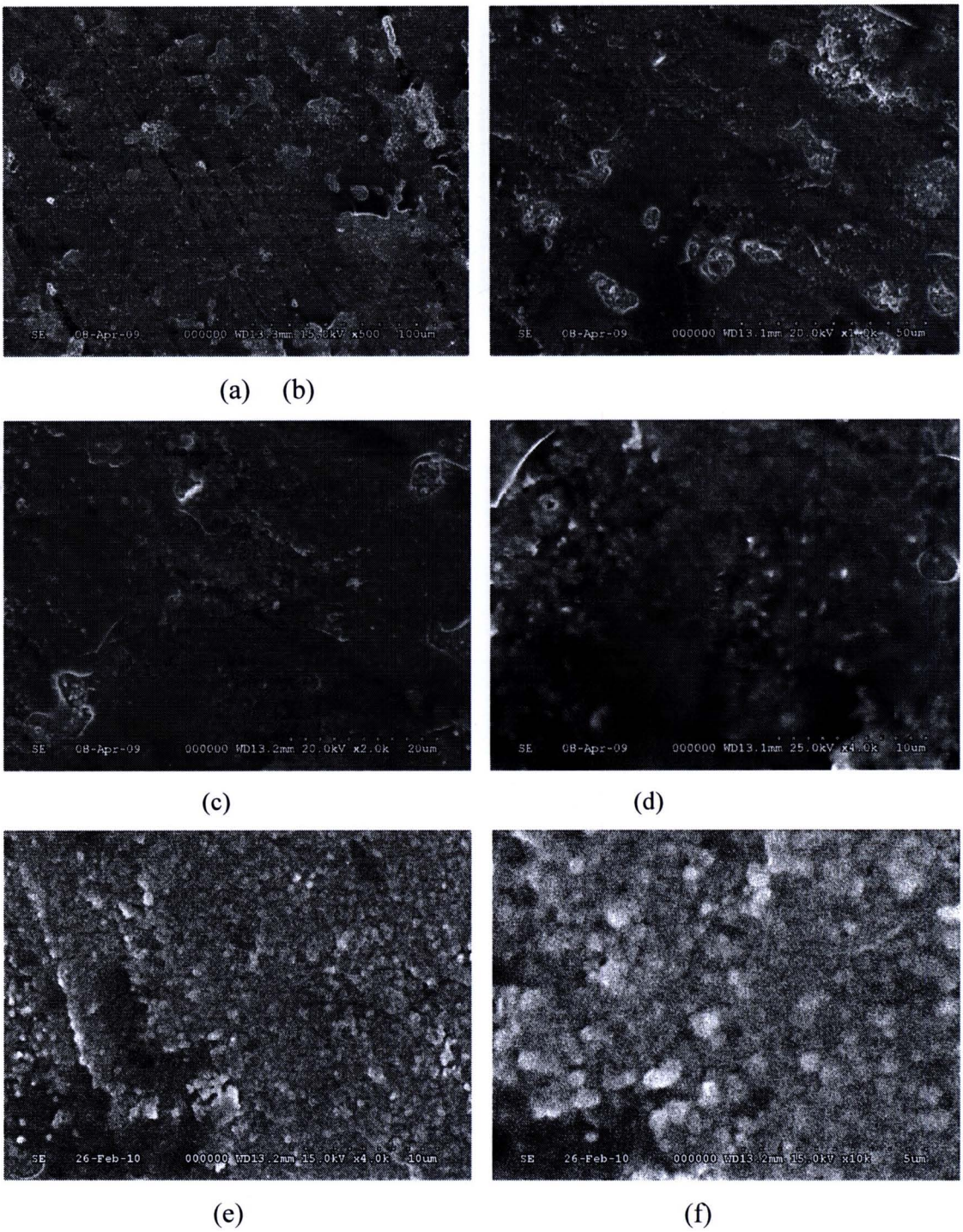

Figure 55 SEM photomicrographs of group VM7 (Cercon®core ceramic veneering with VITA VM7) that reveals fracture core-veneer at the fracture surface of core structure upon (a)X500, (b)X1000, (c)X2000, (d)X4000 magnification and reveals the etched fracture surface of ceramic core at (e)X4000 and (f)X10000 magnification

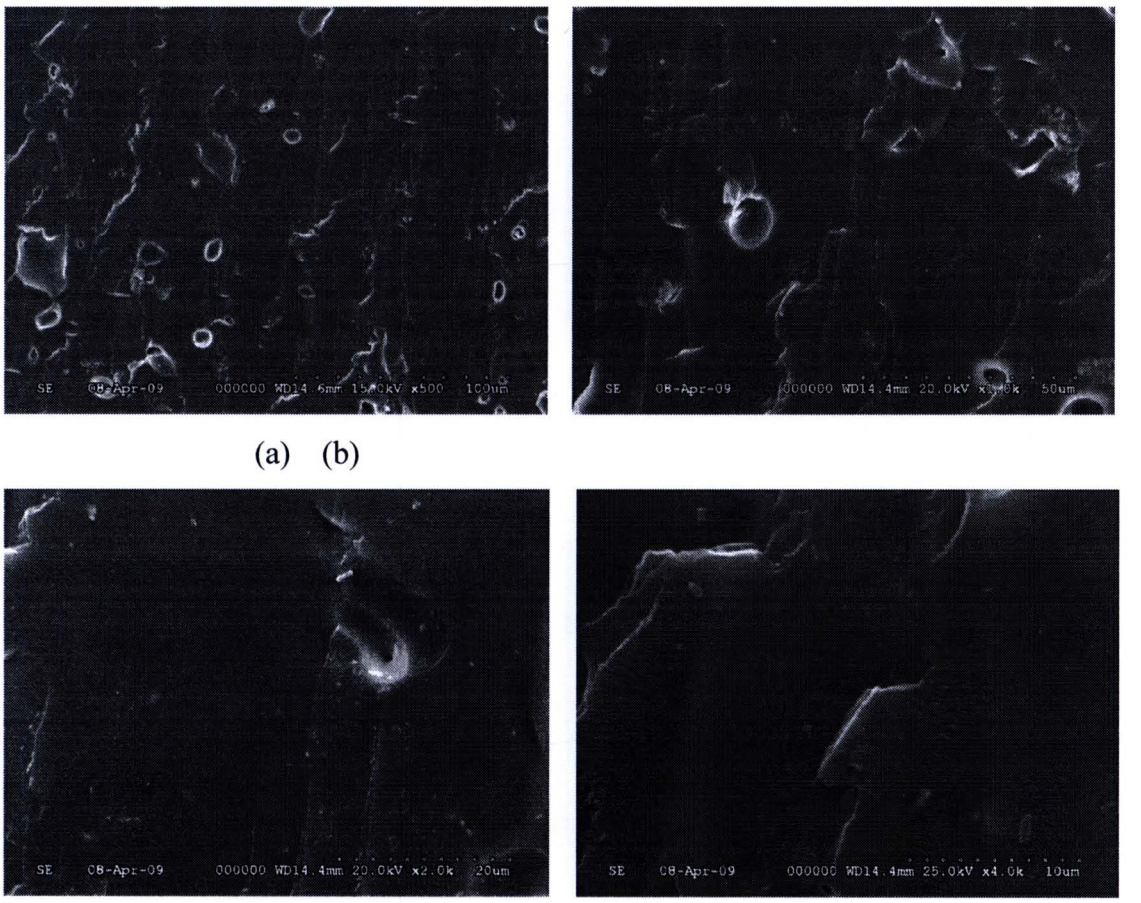

(a) (b)

(c) (d)

Figure 56 SEM photomicrographs of group VM7 (Cercon®core ceramic veneering with VITA VM7) that reveals fracture core-veneer at the fracture surface of VM7 veneering ceramic upon (a)X500, (b)X1000, (c)X2000, (d)X4000 magnification

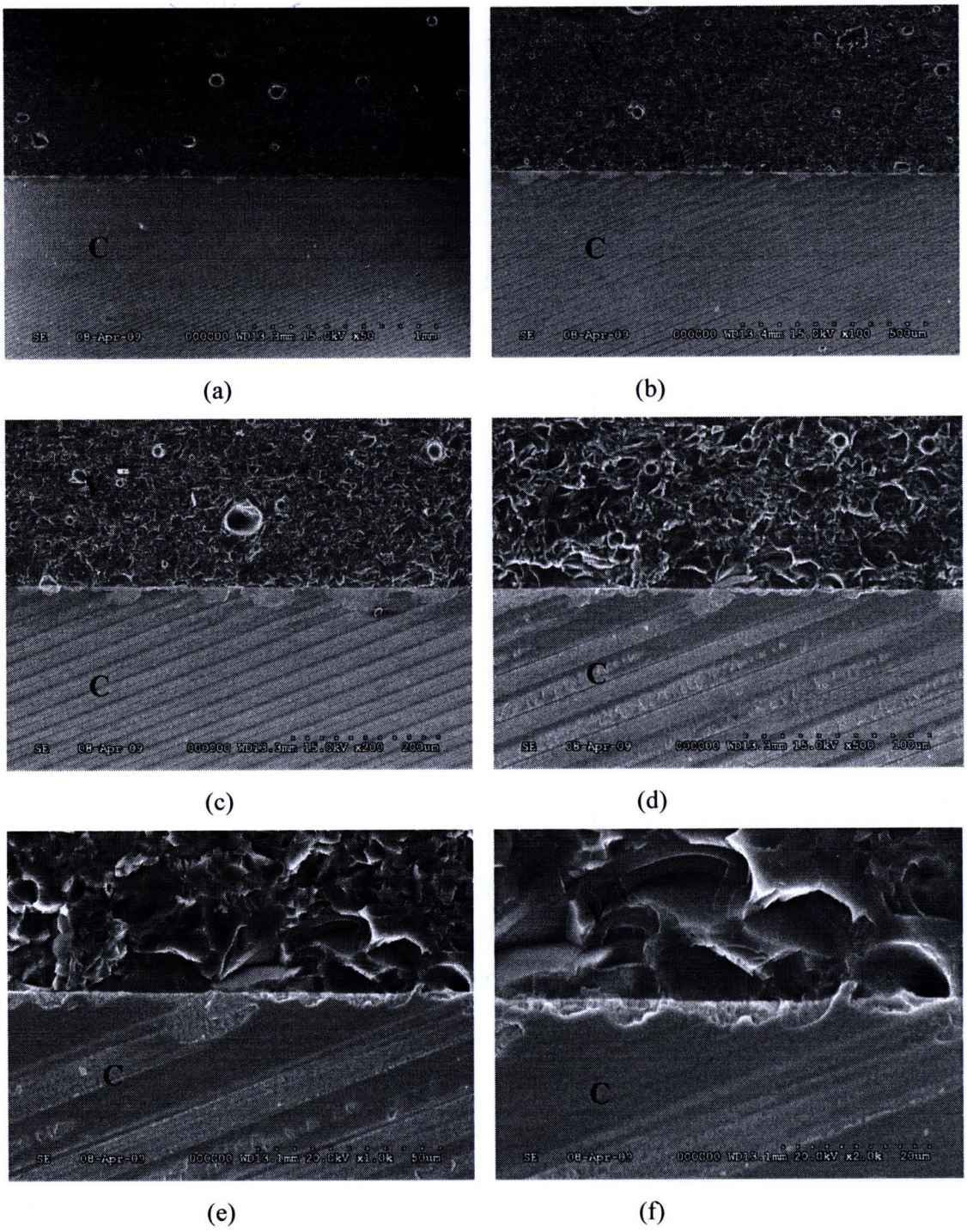

Figure 57 SEM photomicrographs of group VM7 (Cercon®core ceramic veneering with VITA VM7) that reveals the core-veneer interface at (a)X50, (b)X100, (c)X200, (d)X500, (e)X1000, (f)X2000 magnification.

NB: V = Veneering ceramic, C = Cercon® core.

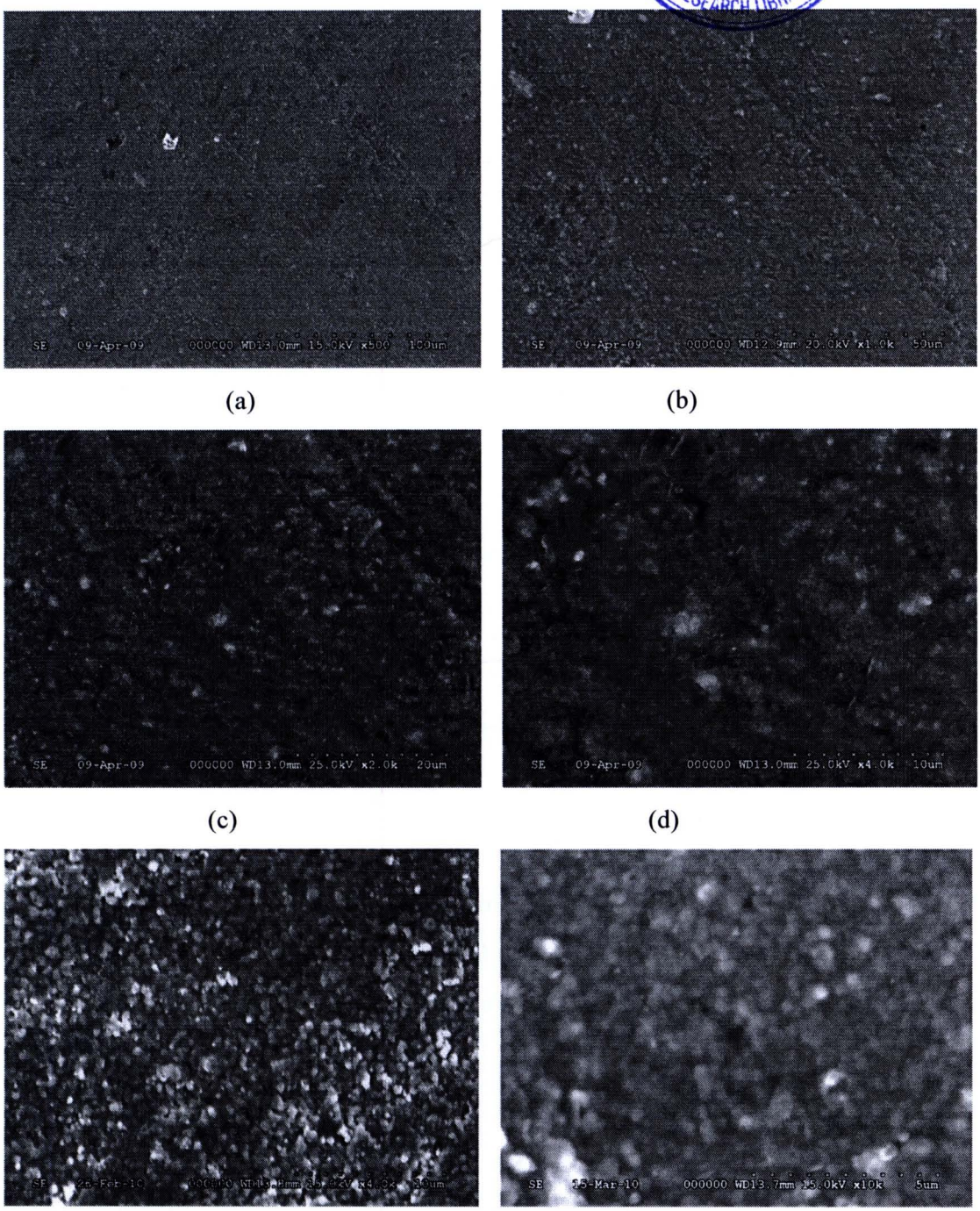

Figure 58 SEM photomicrographs of group VM9 (Cercon®core ceramic veneering with VITA VM9) that reveals fracture core-veneer at the fracture surface of core structure upon (a)X500, (b)X1000, (c)X2000, (d)X4000 magnification and reveals the etched fracture surface of ceramic core at (e)X4000 and (f)X10000 magnification

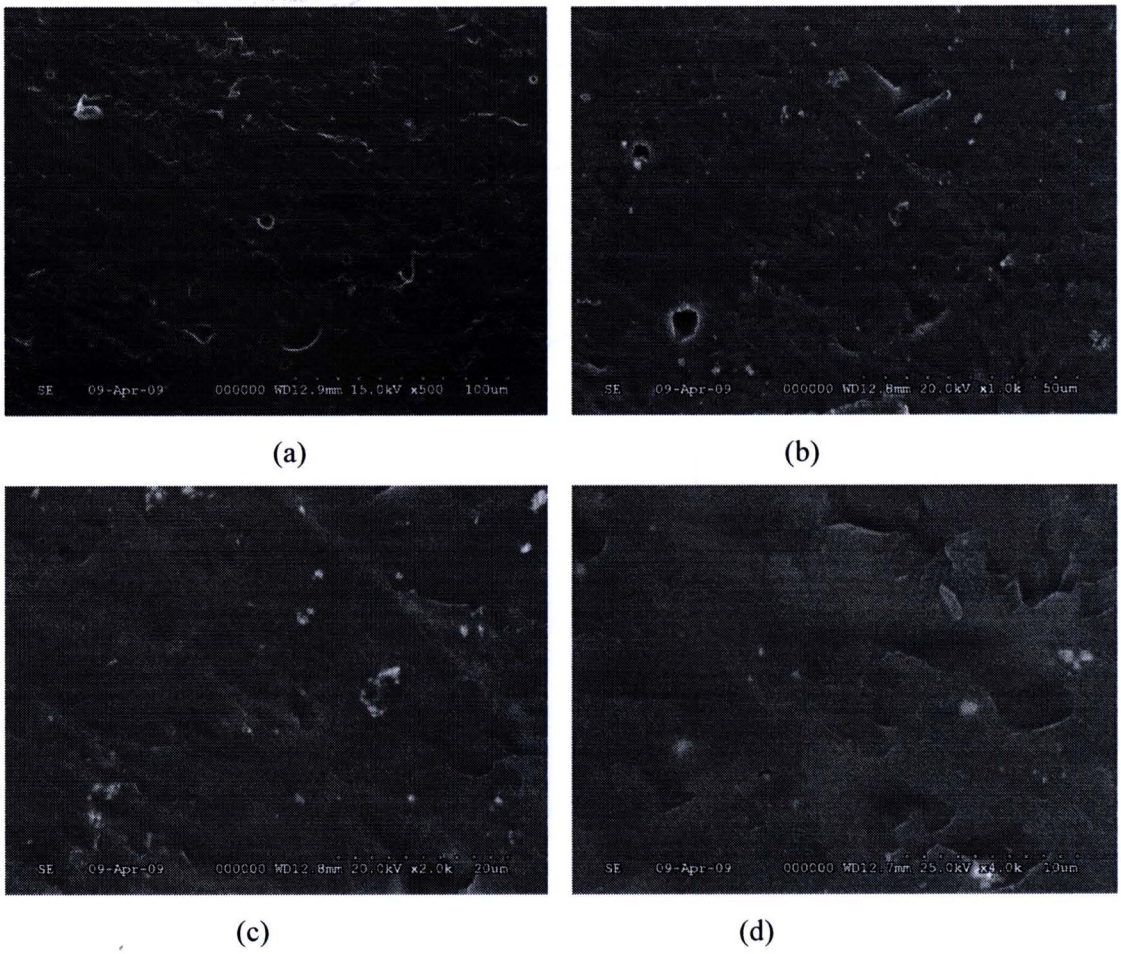

Figure 59 SEM photomicrographs of group VM9 (Cercon®core ceramic veneering with VITA VM9) that reveals fracture core-veneer at the fracture surface of VM9 veneering ceramic upon (a)X500, (b)X1000, (c)X2000, (d)X4000 magnification

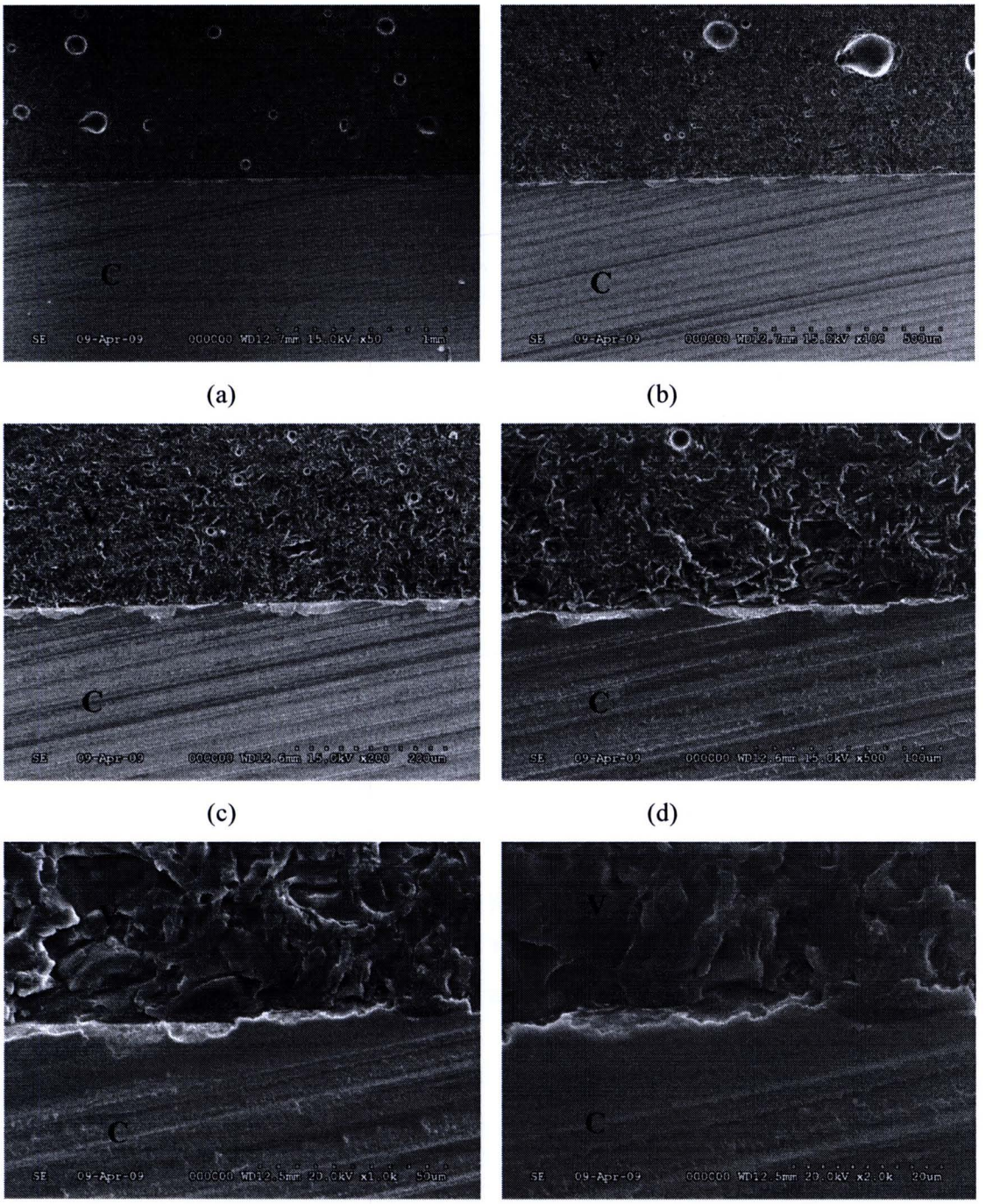

Figure 60 SEM photomicrographs of group VM9 (Cercon® core ceramic veneering with VITA VM9) that reveals the core-veneer interface at (a)X50, (b)X100, (c)X200, (d)X500, (e)X1000, (f)X2000 magnification.

NB: V = Veneering ceramic, C = Cercon® core.

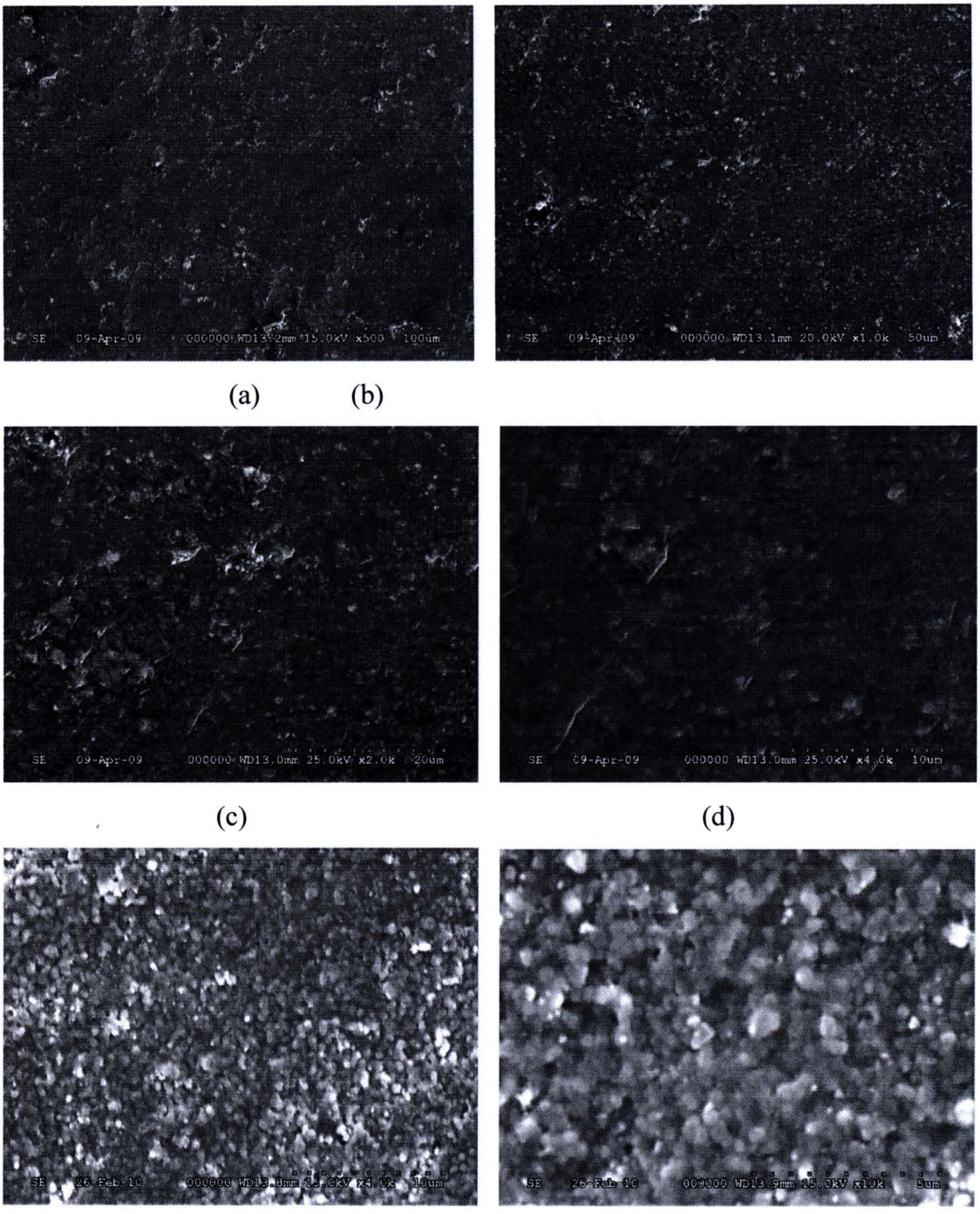

Figure 61 SEM photomicrographs of group CK (Cercon®core ceramic veneering with Cercon ceram kiss) that reveals fracture core-veneer at the fracture surface of core structure upon (a)X500, (b)X1000, (c)X2000, (d)X4000 magnification and reveals the etched fracture surface of ceramic core at (e)X4000 and (f)X10000 magnification

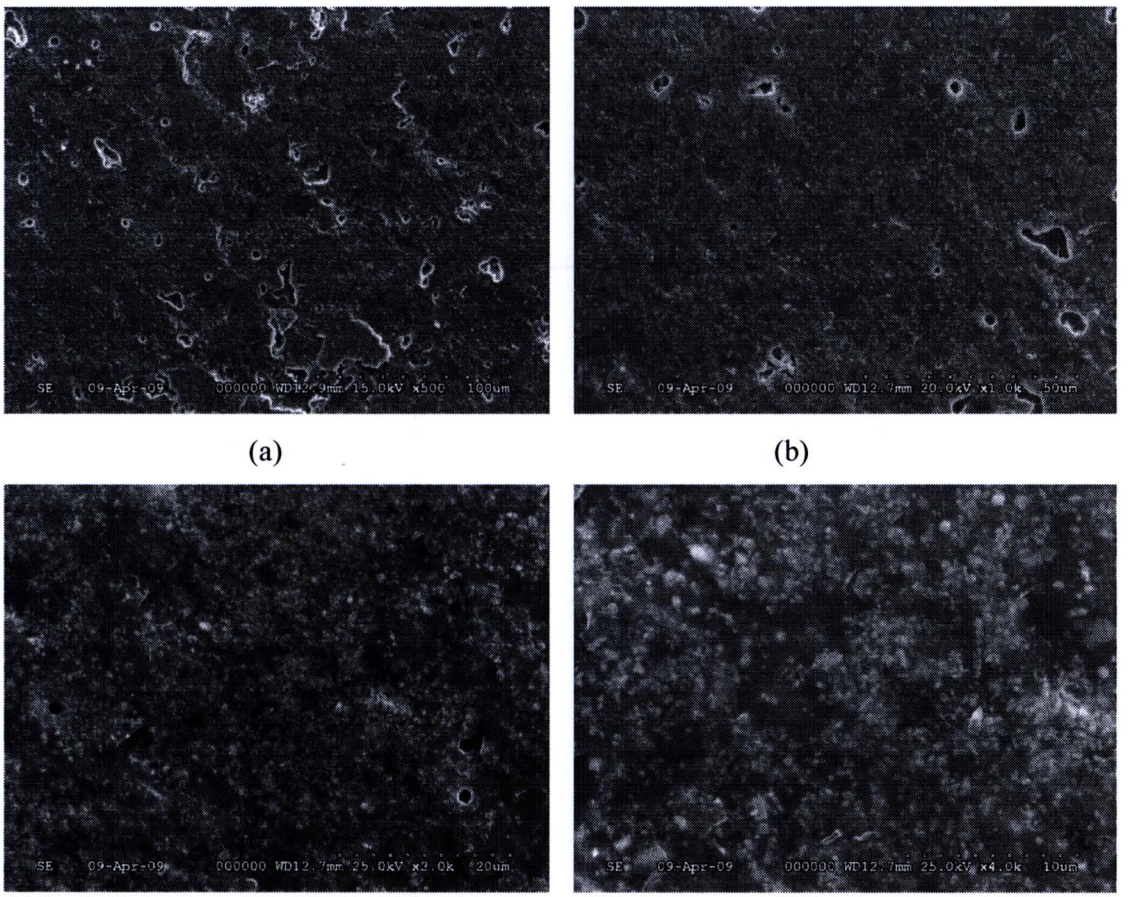

Figure 62 SEM photomicrographs of group CK (Cercon®core ceramic veneering with Cercon ceram kiss) that reveals fracture core-veneer at the fracture surface of CK veneering ceramic upon (a)X500, (b)X1000, (c)X2000, (d)X4000 magnification.

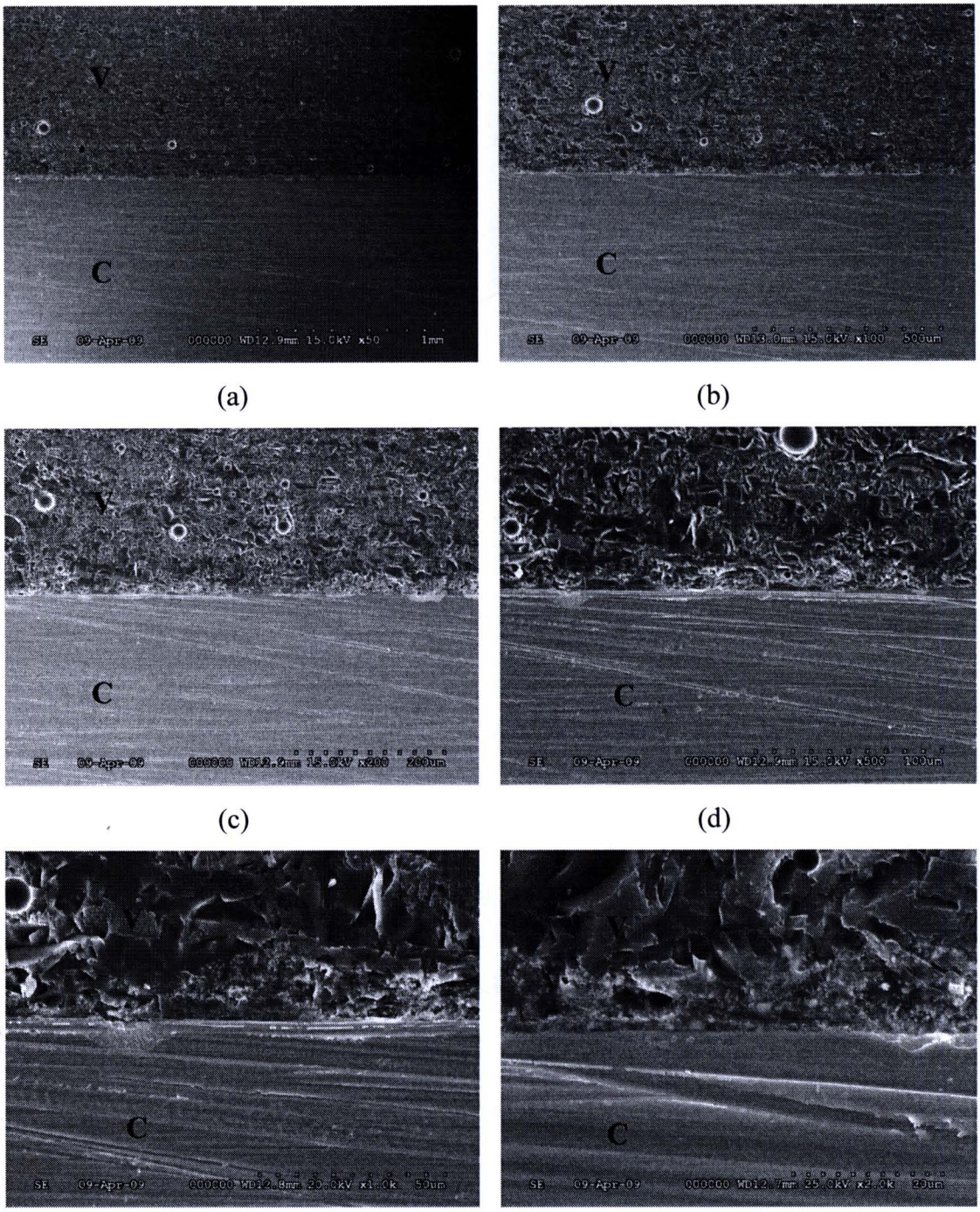

Figure 63 SEM photomicrographs of group CK (Cercon®core ceramic veneering with Cercon ceram kiss) that reveals the core-veneer interface at (a)X50, (b)X100, (c)X200, (d)X500, (e)X1000, (f)X2000 magnification.

NB: V = Veneering ceramic, C = Cercon® core.

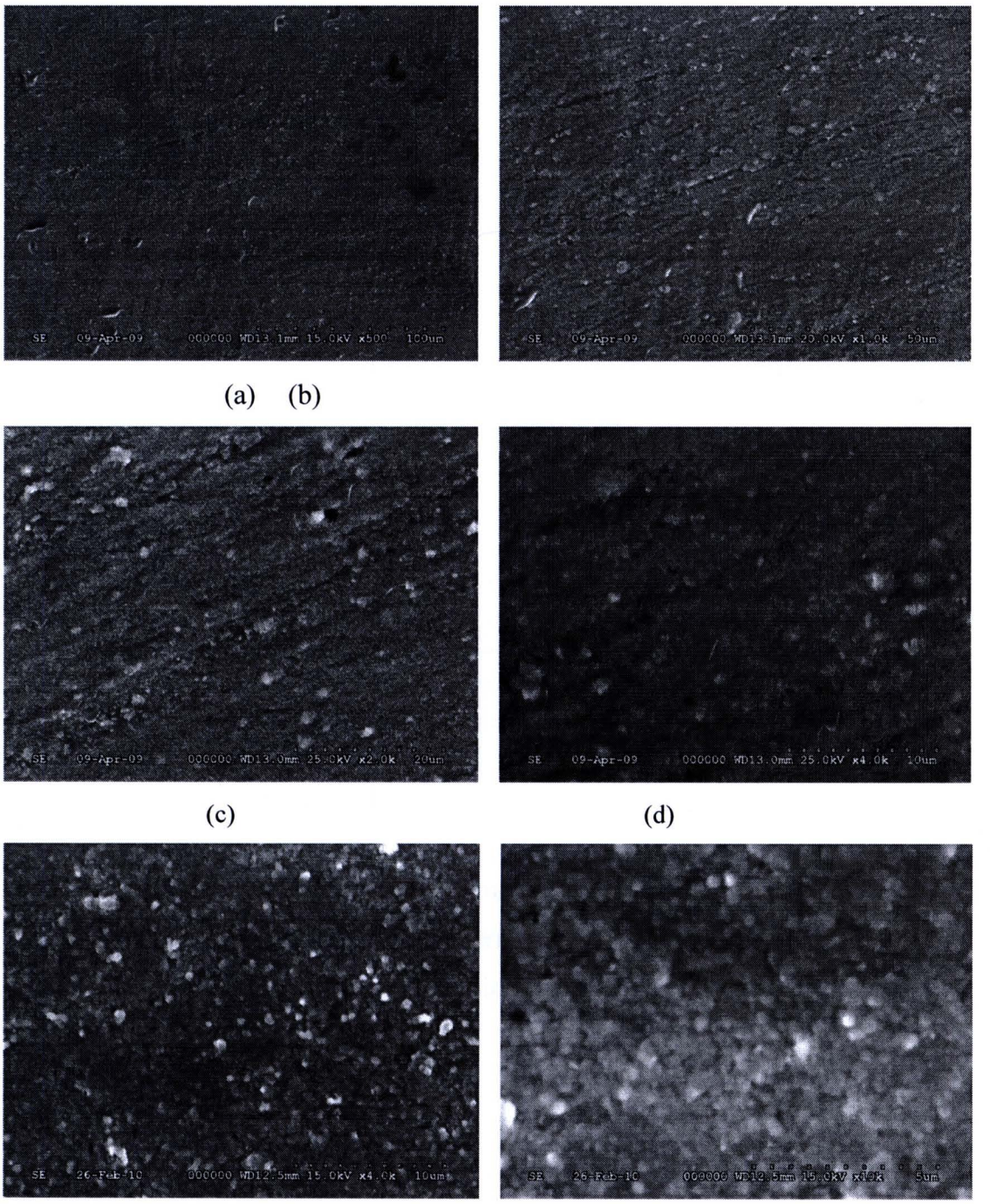

Figure 64 SEM photomicrographs of group emax (Cercon®core ceramic veneering with IPS emax ceram) that reveals fracture core-veneer at the fracture surface of core structure upon (a)X500, (b)X1000, (c)X2000, (d)X4000 magnification and reveals the etched fracture surface of ceramic core at (e)X4000 and (f)X10000 magnification

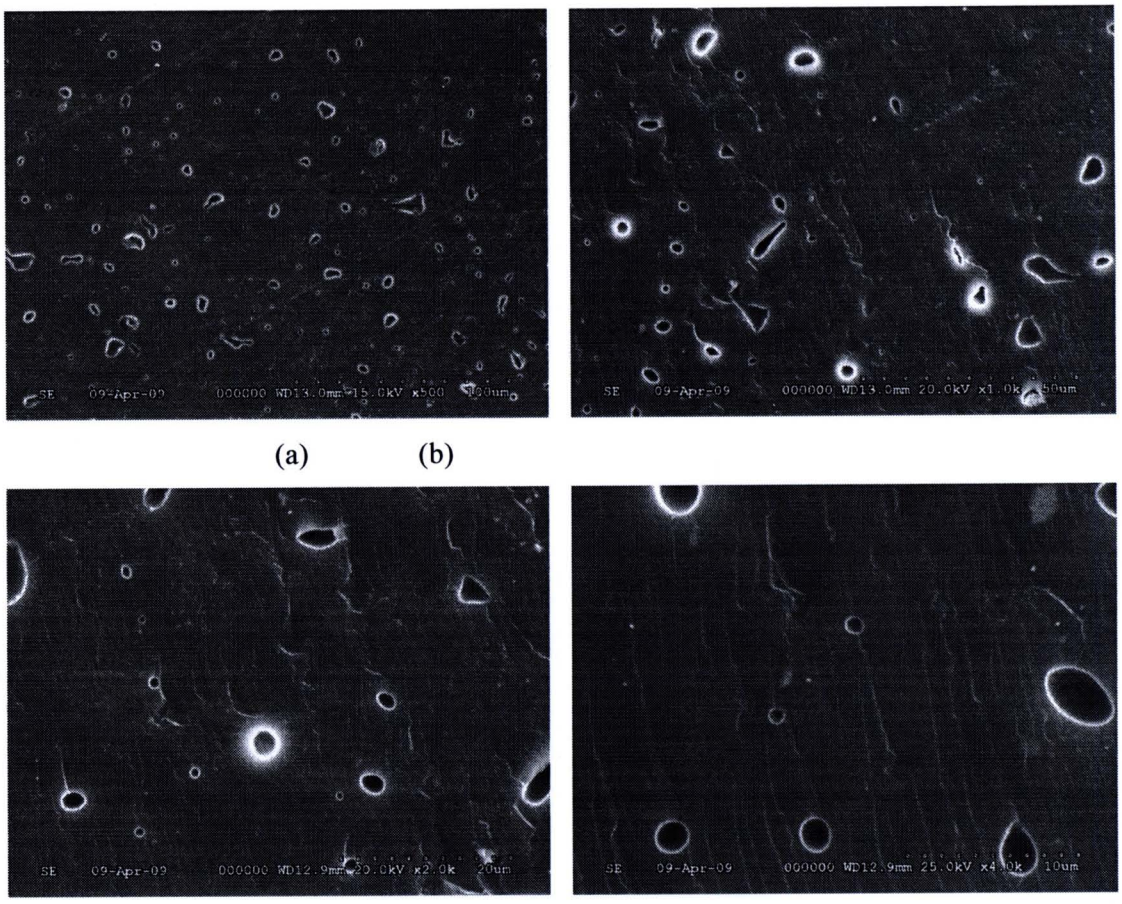

Figure 65 SEM photomicrographs of group emax (Cercon®core ceramic veneering with IPS emax ceram) that reveals fracture core-veneer at the fracture surface of veneering ceramic upon (a)X500, (b)X1000, (c)X2000, (d)X4000 magnification

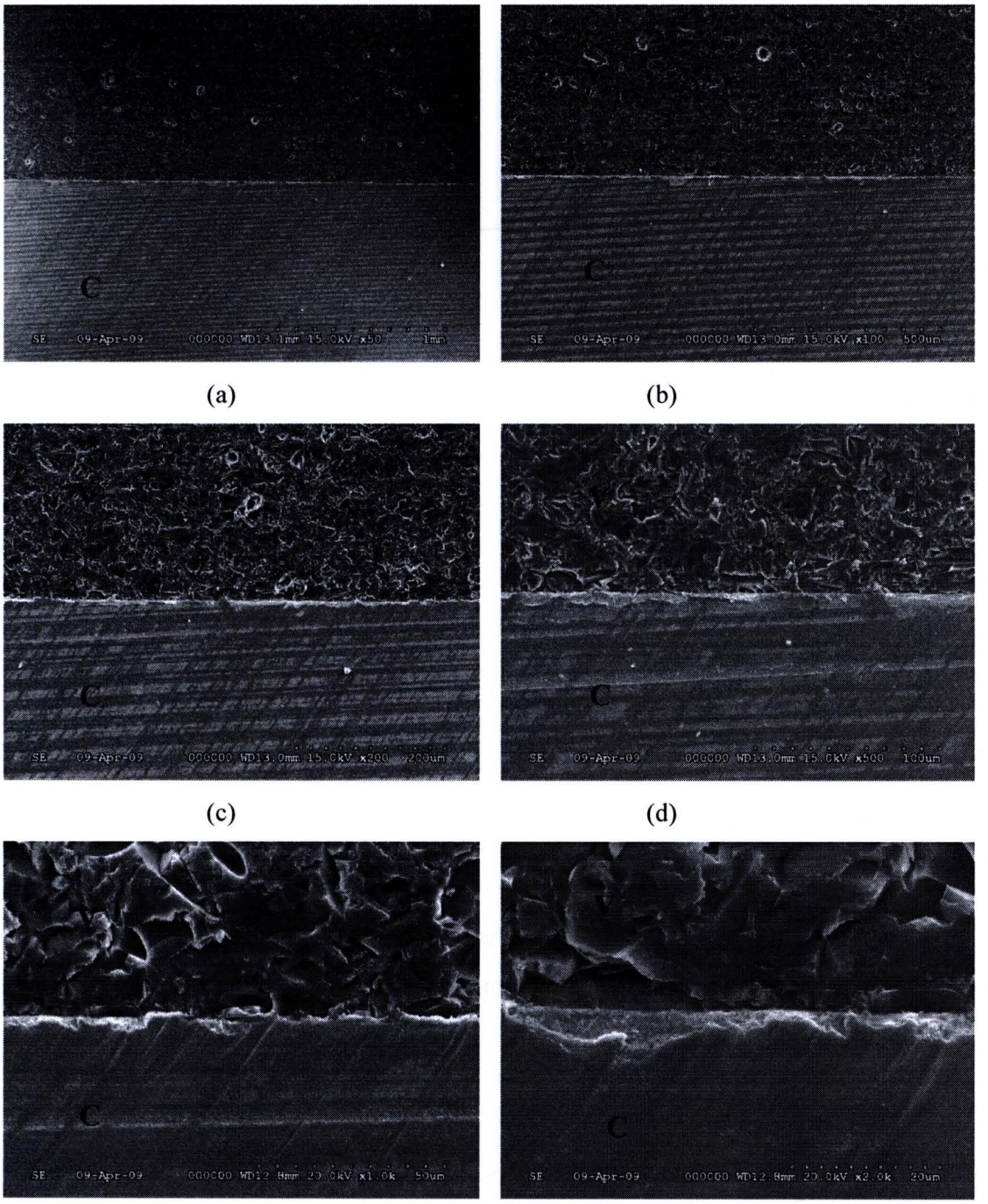

Figure 66 SEM photomicrographs of group emax (Cercon®core ceramic veneering with IPS emax ceram) that reveals the core-veneer interface at (a)X50, (b)X100, (c)X200, (d)X500, (e)X1000, (f)X2000 magnification.

NB: V = Veneering ceramic, C = Cercon® core.

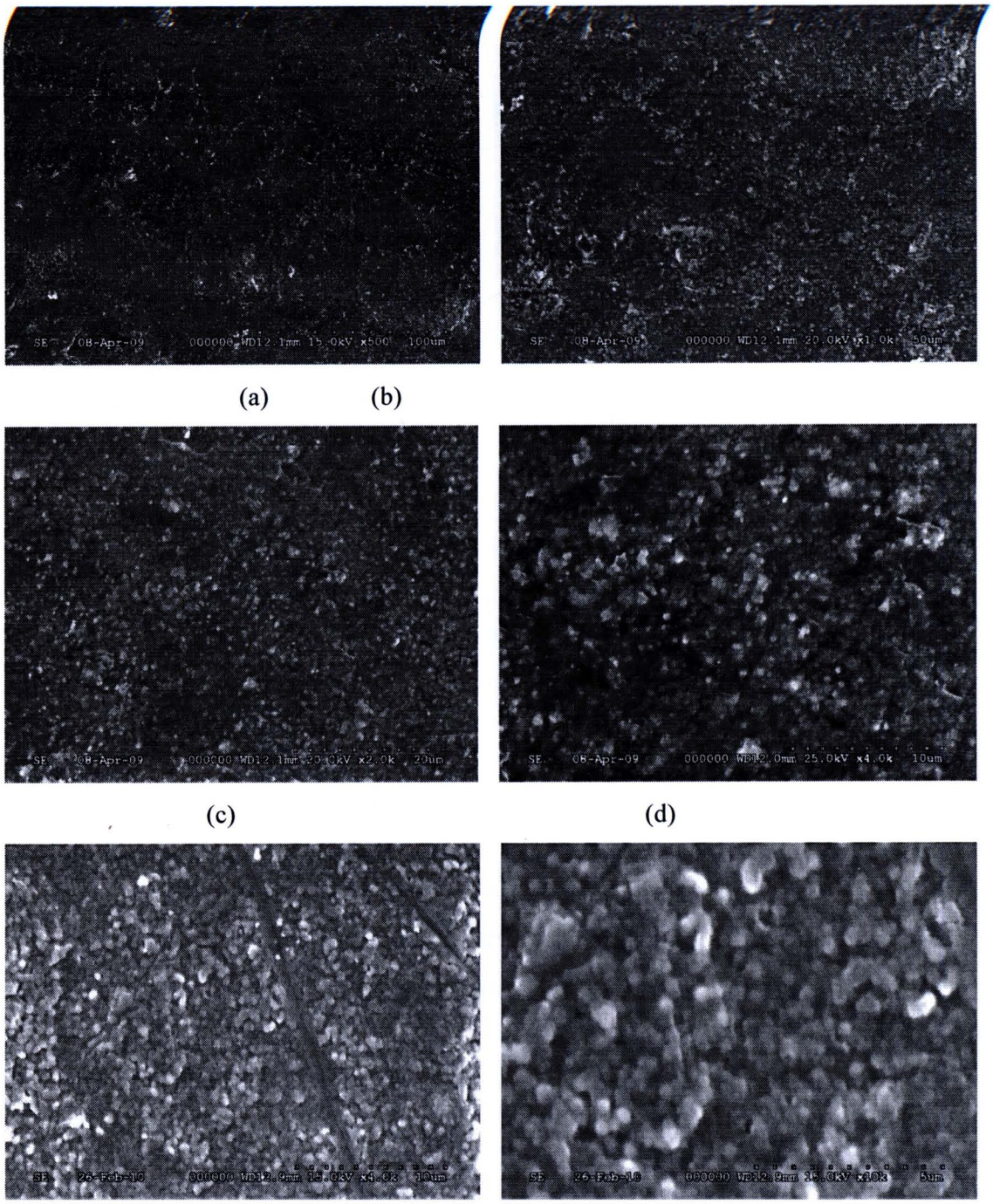

Figure 67 SEM photomicrographs of group dSIGN (Cercon®core ceramic veneering with IPS d Sign) that reveals fracture core-veneer at the fracture surface of core structure upon (a)X500, (b)X1000, (c)X2000, (d)X4000 magnification and reveals the etched fracture surface of ceramic core at (e)X4000 and (f)X10000 magnification

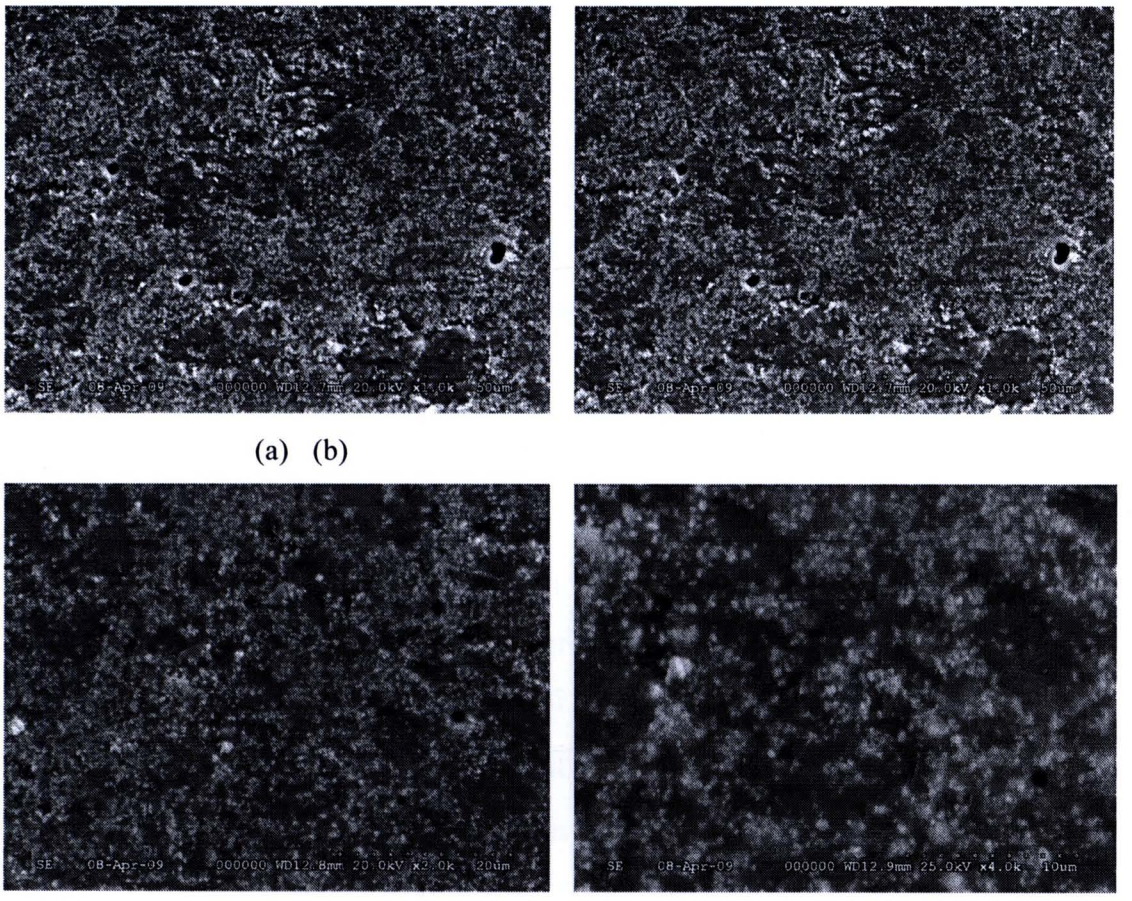

Figure 68 SEM photomicrographs of group dSIGN (Cercon®core ceramic veneering with IPS d Sign) that reveals fracture core-veneer at the fracture surface of veneering ceramic upon (a)X500, (b)X1000, (c)X2000, (d)X4000 magnification

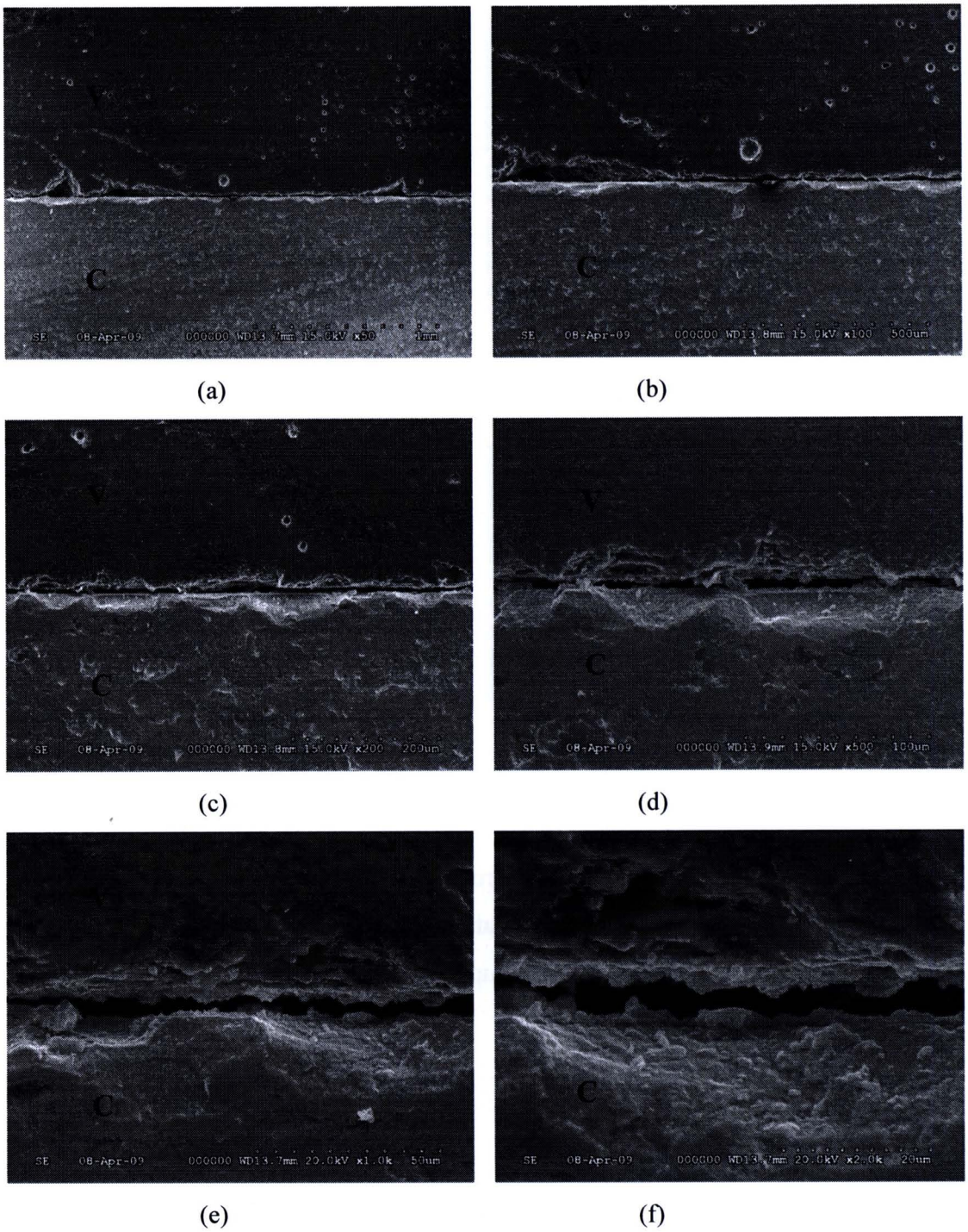

Figure 69 SEM photomicrographs of group dSIGN (Cercon® core ceramic veneering with IPS d Sign) that reveals the core-veneer interface at (a)X50, (b)X100, (c)X200, (d)X500, (e)X1000, (f)X2000 magnification.

NB: V = Veneering ceramic, C = Cercon® core.

4.6 The X-ray diffraction (XRD)

The X-ray diffraction (XRD) is the great importance in the microstructure characterization of complex, multiphase materials. The application of X-ray diffraction methods enables not only qualitative and quantitative phase analysis but also microstructure characterization (crystallite size, lattice distortions, dislocation densities, stacking faults and twins probability)

This study, X-ray diffraction patterns in each group showed that the zirconium oxide, tetragonal phase, was the main crystalline phase using X'Pert Plus crystallographic analysis software. The major peaks of the tetragonal phase were observe at 2θ values of 30.29 ° and 34.75 ° with the dominant peak (highest intensity) at 30.29 °, which corresponded to the (111) crystallographic plane of the tetragonal phase as predicted from the X-ray diffraction standard file (14-0534), the zirconium oxide. The monoclinic phase was detected at 2θ values of 28.75° and 34.75 °, which corresponded to the (111) and (11$\bar{1}$) crystallographic plane as anticipated by the X-ray diffraction standard file (05-0534), the zirconium oxide. The x-ray diffraction patterns were displays in figure 73-79. The x-ray diffraction patterns revealed the major crystalline phase of tetragonal phase with minor amount of monoclinic for all specimens.

The phase analysis was quantified by magnifying the corresponding 2θ range with the X'Pert Plus crystallographic analysis and PCPDFWIN software, subtracting an averaged background line and determining the integral intensities (areas) under the zirconia peaks monoclinic (111), monoclini (11$\bar{1}$) and tetragonal (111). The discrimination of overlapping peaks was done manually. Table 27 shows the relative concentration (in wt.%) of monoclinic zirconia with respect to the total zirconia content and table 28 revealed the transformation of t→m (in wt.%) in each group compared to the Cercon® core specimen that have the major crystalline phase of tetragonal 99.1 % and minor amount of monoclinic 9%.

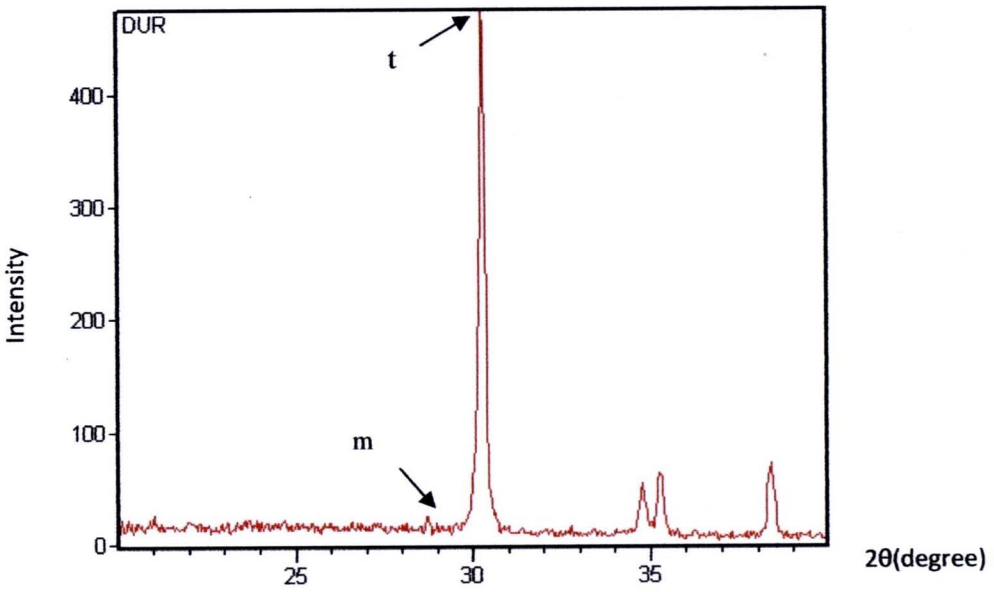

Figure 70 X-ray diffraction (XRD) pattern of Cercon®core of group C-Dur

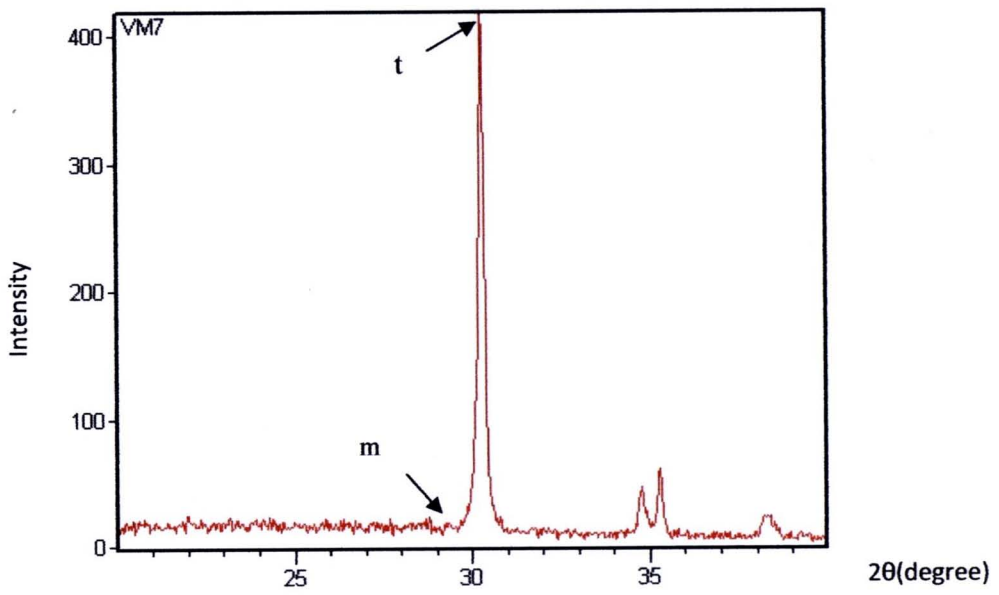

Figure 71 X-ray diffraction (XRD) pattern of Cercon®core of group C-VM7

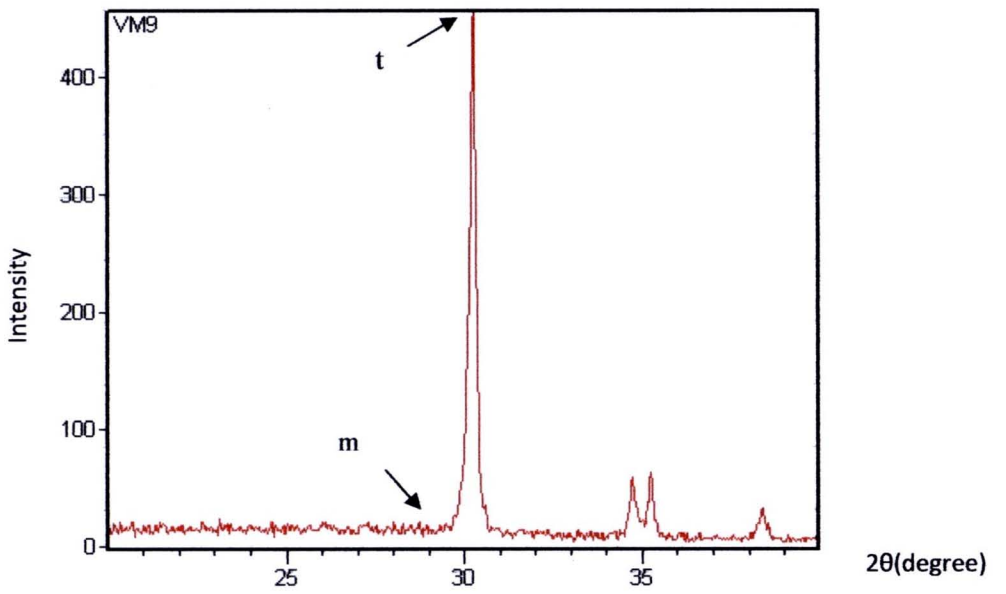

Figure 72 X-ray diffraction (XRD) pattern of Cercon®core of group C-VM9

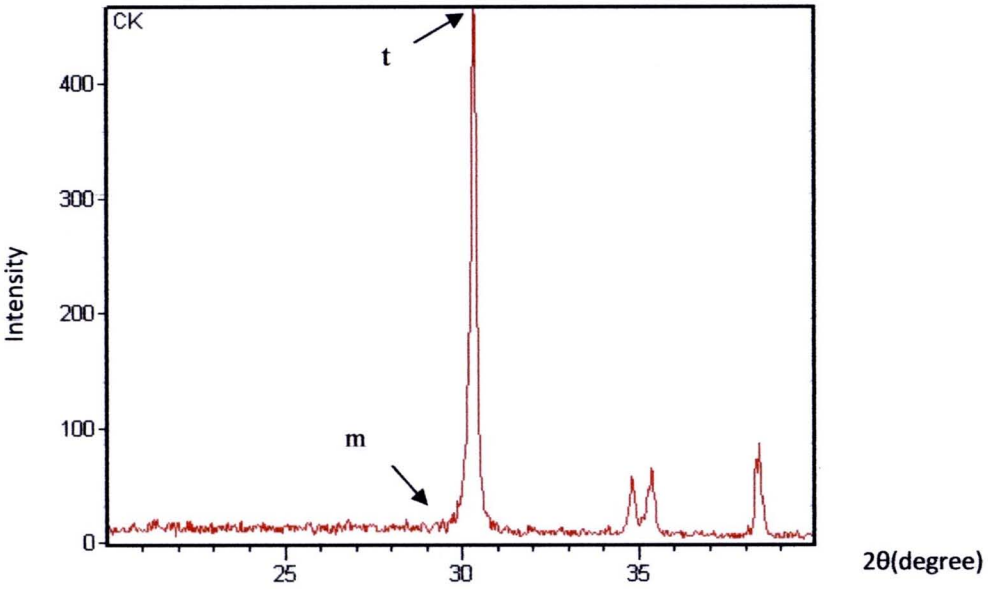

Figure 73 X-ray diffraction (XRD) pattern of Cercon®core of group C-CK

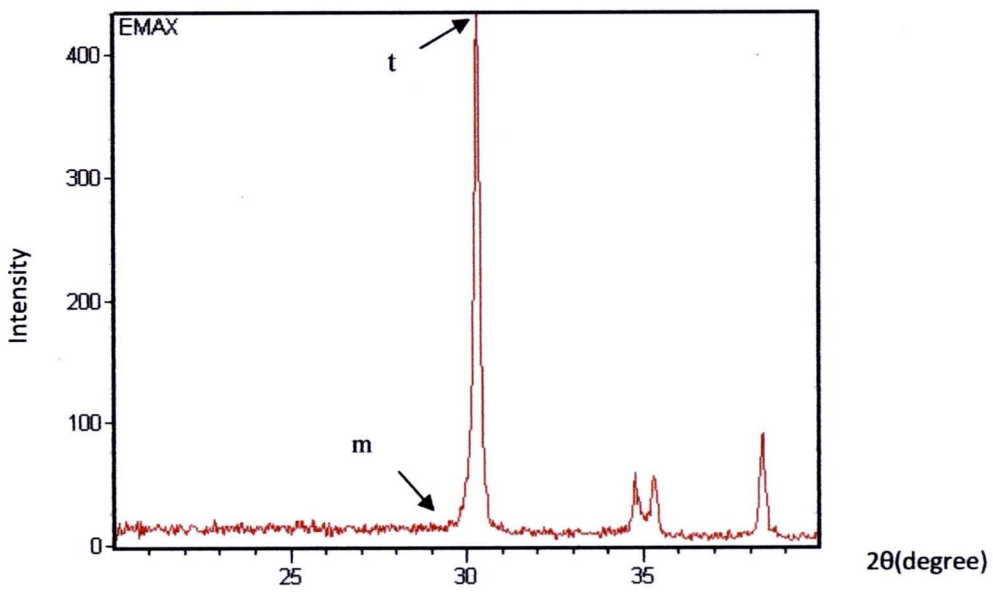

Figure 74 X-ray diffraction (XRD) pattern of Cercon®core of group C-emax

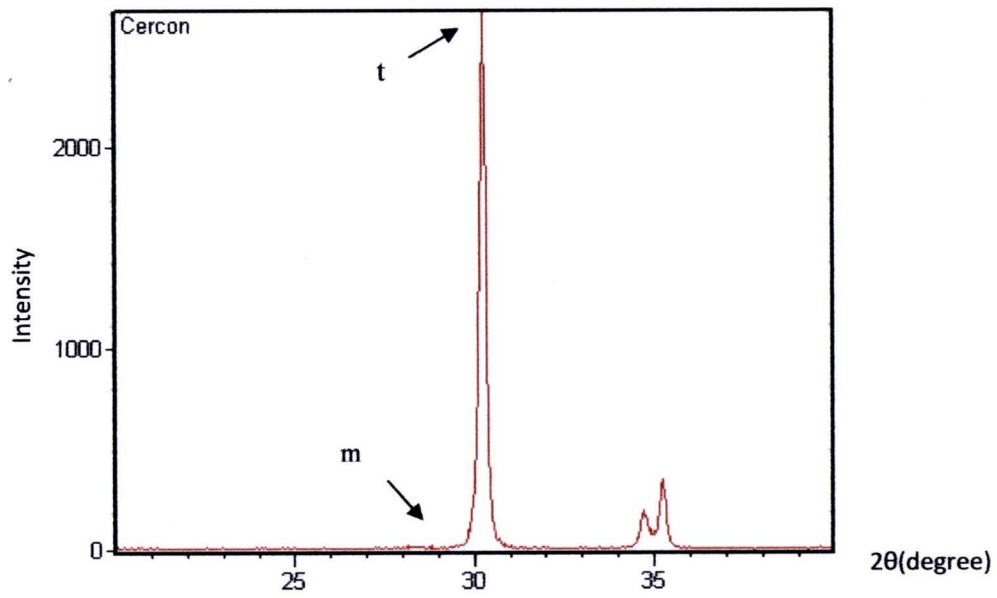

Figure 75 X-ray diffraction (XRD) pattern of Cercon®core ceramic

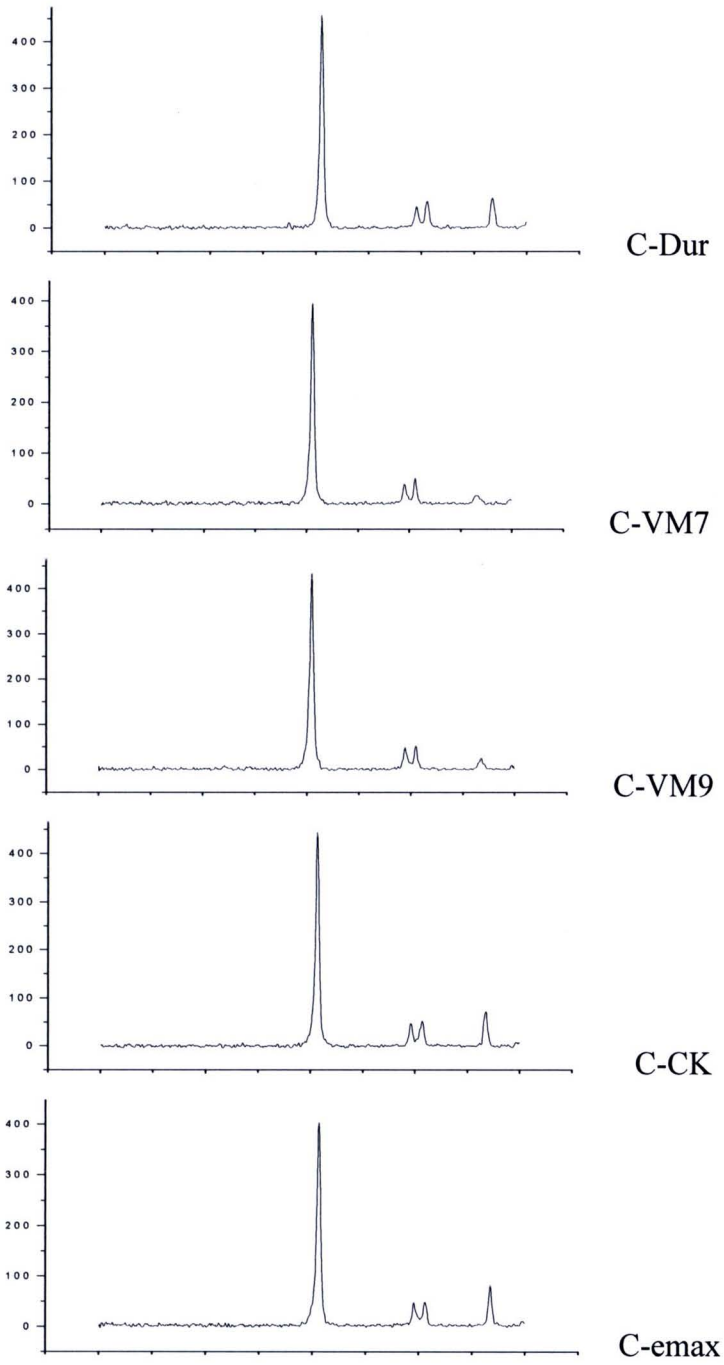

Figure 76 X-ray diffraction(XRD) of Cercon® ceramic of all groups

NB: C = Cercon® core, C-Dur = VITADur® alpha, C-VM7 = VITAVM® 7, C-VM9 = VITAVM® 9, C-CK = Cercon® ceramkiss, C-emax = IPSe.max® ceram.

Table 27 The relative concentration (wt.%) of tetragonal and monoclinic phase of all groups resulting of XRD study

Group	Relative phase concentration (wt.%)	
	Tetragonal phase (t)	Monoclinic phase (m)
C-Dur	0.811	0.189
C-VM7	0.834	0.166
C-VM9	0.784	0.216
C-CK	0.830	0.170
C-emax	0.837	0.163
Cercon®core	0.991	0.009

NB: C = Cercon®core, C-Dur = VITADur® alpha, C-VM7 = VITAVM®7, C-VM9 = VITAVM®9, C-CK = Cercon®ceramkiss, C-emax = IPSe.max®ceram.

Table 28 The relative concentration (wt.%) of t→m phase transformation in each group compared to Cercon®core

Group	Relative concentration (wt.%) of t→m
C-Dur	18.0
C-VM7	15.7
C-VM9	20.7
C-CK	16.1
C-emax	15.4

NB: C = Cercon®core, C-Dur = VITADur® alpha, C-VM7 = VITAVM®7, C-VM9 = VITAVM®9, C-CK = Cercon®ceramkiss, C-emax = IPSe.max®ceram.